

Stripes in oxygen-enriched cuprates

Manfred Bucher

Physics Department, California State University, Fresno,
Fresno, California 93740-8031

(Dated: October 11, 2020)

Abstract

Charge-order stripes of different types occur when copper oxides are doped with either heterovalent metal, like $La_{2-x}Sr_xCuO_4$, or oxygen doped, like $YBa_2Cu_3O_{6+y}$. The difference shows up in the doping dependence of their incommensurability: $q_c(x) \propto \sqrt{x - \tilde{p}}$ but $q_c(y) \approx 0.3$. The square-root dependence in the former compound family results from Coulomb repulsion between doped holes (or electrons), residing pairwise in lattice-site O (or Cu) atoms of the CuO_2 planes. The almost constant $q_c(y)$ value in the second family results from the aggregation of ozone-like molecules, formed from O^{2-} ions of the host with embedded oxygen atoms, $\overset{\circ}{O}$, at interstitial sites in the CuO_2 planes. The magnetic moments, $\mathbf{m}(O)$, of the lattice-defect O atoms in the first family arrange antiferromagnetically, which gives rise to accompanying magnetization stripes of incommensurability $q_m(x) = \frac{1}{2}q_c(x)$. The ozone complexes have a vanishing magnetic moment, $\mathbf{m} = 0$, which explains the absence of accompanying magnetization stripes in the second family. Embedding excess oxygen as $\overset{\circ}{O}$ atoms in CuO_2 planes is likewise assumed for $HgBa_2CuO_{4+\delta}$ and oxygen-enriched bismuth cuprates. A combination of characteristics from both families is present in oxygen-enriched La_2CuO_{4+y} . The validity of determining the hole density in oxygen-enriched cuprates with the universal-dome method is independently confirmed. Besides causing different types of stripes, the two types of lattice-defect oxygen may also cause different types of superconductivity. This could explain the much higher $T_{c,max}$ in oxygen-enriched than Ae -doped cuprates, as well as the cusped cooling-curves of X-ray intensity diffracted by stripes in the former family.

I. INTRODUCTION

Two types of charge-order stripes are observed in copper oxides of high transition temperature (“high- T_c ”) superconductivity. The distinction is characterized by the doping dependence of their incommensurability and is determined by the doping species—whether doped with heterovalent metal or oxygen. Doping with heterovalent metal results in hole doping when divalent alkaline earth ions, $Ae^{2+} = Sr^{2+}, Ba^{2+}$, partially substitute trivalent lanthanide ions, $Ln^{3+} = La^{3+}, Nd^{3+}$, but in electron doping by substitution with tetravalent cerium, Ce^{4+} . Examples are $La_{2-x}Ae_xCuO_4$ and $Nd_{2-x}Ce_xCuO_4$. All compounds of this family have the ‘214’ crystal structure (of T or T’ type). Examples of oxygen doping (or enrichment) are $YBa_2Cu_3O_{6+y}$, $HgBa_2CuO_{4+\delta}$, $Bi_2Sr_{2-x}La_xCuO_{6+\delta}$ and $Bi_2Sr_2CaCu_2O_{8+\delta}$. Common to both families is the presence of CuO_2 planes where the stripes reside (and where superconductivity occurs). However, the doping dependence of their stripe incommensurability is distinctly different: For the family of the ‘214’ compounds it is given, in reciprocal lattice units (r.l.u.), by

$$q_c(x) = \frac{\Omega^\pm}{2} \sqrt{x - \check{p}}, \quad x \leq \hat{x}, \quad (1)$$

for Ae doping x up to a “watershed” value \hat{x} .¹ The stripe-orientation factor is $\Omega^+ = \sqrt{2}$ for $x > 0.056$ when stripes are parallel to the a or b axis, but $\Omega^- = 1$ for $x < x_6$ when stripes are diagonal. The offset value under the radical is $\check{p} \leq 0.02$ for the hole-doped ‘214’ compounds. A qualitative change of the incommensurability occurs at a watershed concentration of the dopant, \hat{x} , which depends on the species of doping and co-doping. It shows up as *kinks* in the $q_c(x)$ profile at \hat{x} (see Fig. 1), where the square-root curve from Eq.(1) levels off to constant plateaus,

$$q_c(x) = \frac{\sqrt{2}}{2} \sqrt{\hat{x} - \check{p}}, \quad x > \hat{x}. \quad (2)$$

The charge-order stripes in the ‘214’ family are accompanied by magnetization stripes of incommensurability

$$q_m(x) = \frac{1}{2} q_c(x). \quad (3)$$

In stark contrast, the incommensurability of charge-order stripes in $YBa_2Cu_3O_{6+y}$ —and similarly in the oxygen-enriched Hg and Bi compounds—depends only weakly on oxygen doping, $q_c(y) \approx 0.3$, *decreasing* slightly with super-oxygenation (see Fig. 1). Noticeably, those stripes are *not* accompanied (at the same doping y) by magnetization stripes. A re-

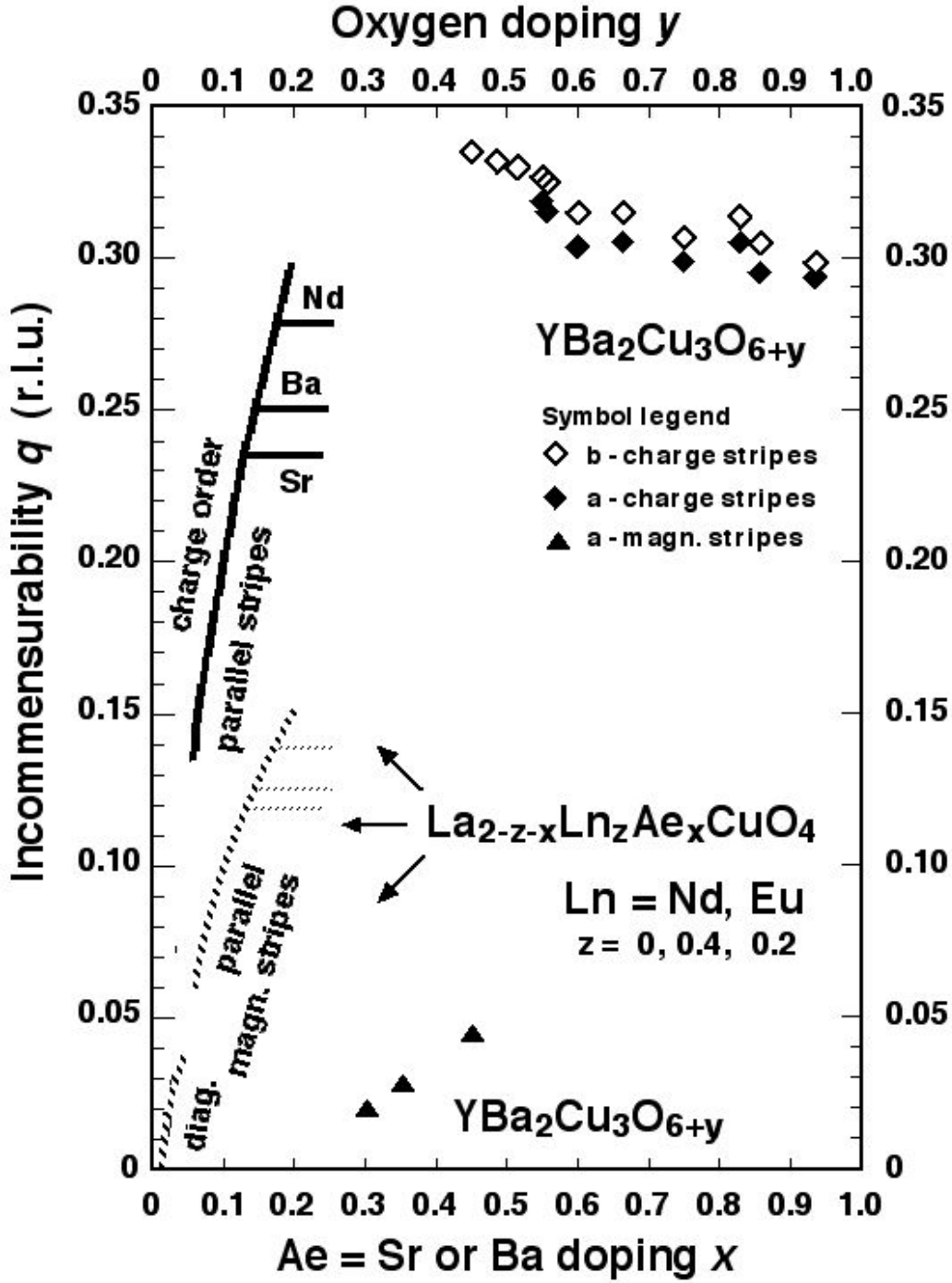
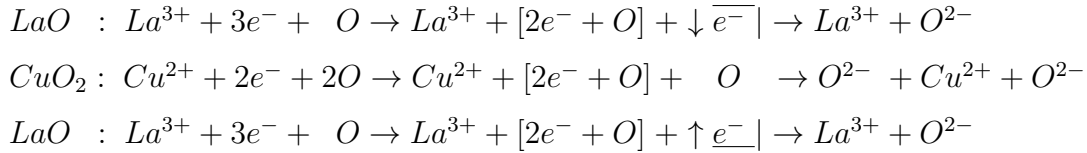


FIG. 1. Incommensurability of charge-order stripes (solid line) and magnetization stripes (hatched line) in $La_{2-z-x}Ln_zAe_xCuO_4$ of the ‘214’ family due to Ae doping with $Ae = Sr$ or Ba (curves on the left) and in oxygen-doped $YBa_2Cu_3O_{6+y}$ (data from Refs. 2-17) near the top and bottom. The curves are graphs of Eqs. (1-3). The discontinuity at $x = 0.056$ is caused by a change of stripe orientation from diagonal to parallel, relative to the $Cu-O$ bonds.

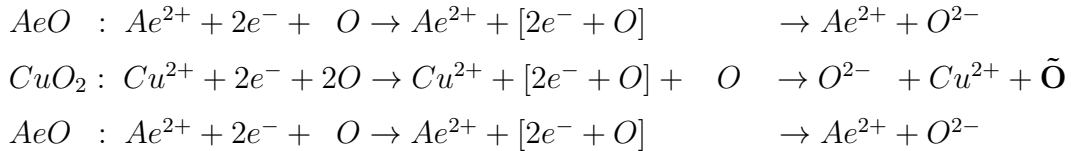
sult of insufficient annealing,⁶ magnetization stripes of square-root doping dependence, akin to Eq. (1), have been observed in $YBa_2Cu_3O_{6+y}$ in the middle range of oxygen doping,⁵ $0.30 \leq y \leq 0.45$, preceding the doping range of charge-order stripes, $0.45 \leq y \leq 0.92$. Since the incommensurability is much better understood in the *Ae*-doped ‘214’ compounds¹ than in the oxygen-doped cuprates, knowledge about the former can be used to make inferences about the observed similarities and differences with stripes in the latter family. This is the aim of the present paper. To this end the nature of stripes in the ‘214’ family is briefly reviewed.

II. STRIPES IN LANTHANUM CUPRATES DOPED WITH ALKALINE-EARTH

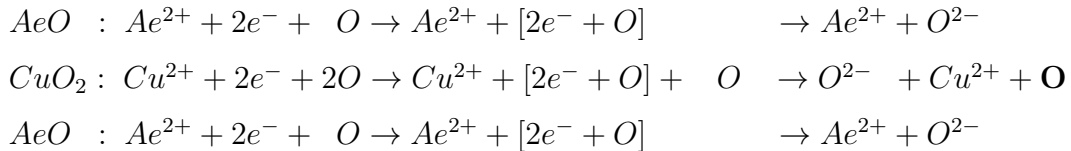
The unit cell of *pristine* La_2CuO_4 has a central CuO_2 plane, sandwiched by LaO planes (see Fig. 2). Consider stepwise ionization, where brackets indicate electron localization at atoms, both within the planes and by transfer from the LaO planes to the CuO_2 plane:



In the simplest case of *doping*, *Ae* substitutes, in some cells, *La* in both sandwiching planes:



The lack of electron transfer from the sandwiching planes to the CuO_2 plane leaves some oxygen atoms *neutral* (marked bold above and below). Compared to the host crystal, they can be regarded as housing the holes (pairwise). Up to a density $\check{p} \leq 0.02$, such holes are *itinerant*, enabling $\tilde{\mathbf{O}}$ atoms to skirmish long-range antiferromagnetism (3D-AFM). The remaining lack of electron transfer leaves more oxygen atoms *stationary* at lattice sites, \mathbf{O} . They give rise to static stripes (to be explained instantly).

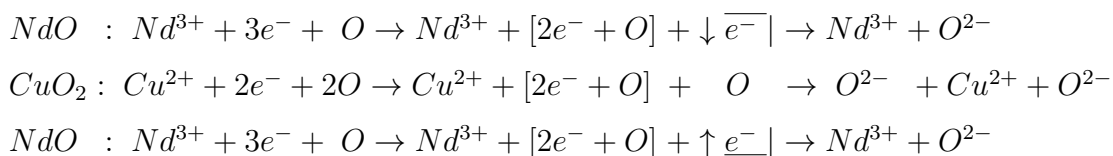


Relative to the host crystal, both the skirmishing and stationary oxygen atoms, \tilde{O} and O , appear positive, holding two elementary charges, $+2|e|$, each (see Appendix A). In this sense, the doping of La_2CuO_4 with Ae is often called “hole doping” (more accurately, doping the CuO_2 planes with holes). Both the \tilde{O} and O atoms have a finite magnetic moment, $\mathbf{m}(\tilde{O}) = \mathbf{m}(O) \neq 0$, due to their spin quantum number $S = 2 \times \frac{1}{2} = 1$ according to the spin configuration $[\uparrow\downarrow] [\uparrow] [\uparrow]$ of their $2p^4$ subshell (Hund’s rule of maximal multiplicity). The moments of the skirmishing oxygen atoms, $\mathbf{m}(\tilde{O})$ —itinerant *via* anion lattice sites—upset the 3D-AFM the host [from $\mathbf{m}(Cu^{2+})$ moments] and cause its collapse at hole density $\check{p} = 0.02$ (more in Sect. V).

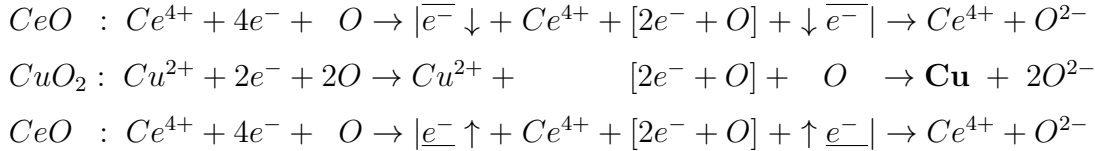
The superlattice, formed by the O ions, gives rise to charge-order stripes and magnetization stripes with a square-root dependence of the incommensurability on doping, Eqs. (1, 3). The square-root dependence of $q_c(x)$ results from the spreading of the double holes by Coulomb repulsion to the farthest available separations. Thus a rising square-root profile of stripe incommensurability signifies an underlying superlattice of *lattice-defect charges* (relative to the host crystal). The charge-order and magnetization stripes are coupled, Eq. (3), because the constituting charges and magnetic moments reside at the *same sites*—the lattice-defect O atoms. It is the antiparallel orientation of neighboring magnetic moments $\mathbf{m}(O)$ —in the O superlattice—that doubles the periodic length of the magnetization stripes. Increasing density of the doped holes, housing pairwise at lattice-defect O atoms in the CuO_2 planes, raises their Coulomb repulsion energy. When doping exceeds a watershed value, $x > \hat{x}$, additional holes overflow to the LaO planes¹ where they also reside pairwise in O atoms. This leaves charge-order stripes of *constant* q_c in the CuO_2 planes, Eq. (2).

III. STRIPES IN n-DOPED $Nd_{2-x}Ce_xCuO_{4+\delta}$ AND OXYGENATED $La_2CuO_{4+\delta}$

The unit cell of *pristine* Nd_2CuO_4 has a central CuO_2 plane, sandwiched by NdO planes, analogous to La_2CuO_4 in Fig. 2. Consider again crystal formation by stepwise ionization, where brackets indicate electron localization at atoms, both within the planes and by transfer from the NdO planes to the CuO_2 plane:



In the simplest case of *doping*, *Ce* substitutes, in some cells, *Nd* in both sandwiching planes:



Doping lanthanide-based cuprates with cerium, $Ln_{2-x}Ce_xCuO_{4+\delta}$ ($Ln = Nd, Pr, La, Sm, Eu$), partially substitutes Ln^{3+} by Ce^{4+} , resulting in *electron doping* of the CuO_2 planes. The doped electrons reside pairwise in lattice-site \mathbf{Cu} atoms.¹ For reasons of stability, the crystals need to be grown with excess oxygen, O_δ , to be eliminated in post-growth annealing.¹⁸ The incommensurability of charge-order stripes (for $x > x_6$) is given by Eq. (1) with $\tilde{p} = 2\delta$.¹ As Eq. (1) is based on Coulomb repulsion of like charges in the CuO_2 planes, its success for stripes in electron-doped ‘214’ compounds (of T’ structure) implies that the excess oxygen must reside interstitially as oxygen *ions*, O_δ^{2-} , in or between the LnO planes (see Fig. 2).¹ It results in a *hole-doping* contribution to the CuO_2 planes that correspondingly reduces their electron-doping from *Ce*. Onset of superconductivity in nominal $Nd_{2-x}Ce_xCuO_4$ is observed at *Ce* doping $x \simeq 0.13$.¹⁸ However, recent experiments have shown onset of superconductivity at much lower x when additional electron doping is accomplished by *oxygen deficiency*, $Nd_{2-x}Ce_xCuO_{4-\delta}$.¹⁹

Concerning the Mott insulator La_2CuO_4 , superconductivity is achieved not only by doping with heterovalent metal, $La_{2-x}M_xCuO_4$ ($M = Sr, Ba, Ce$), but also by *oxygen enrichment*, $La_2CuO_{4+\delta}$. However, there are notable differences. Investigations with neutron scattering and X-ray spectroscopy have shown that $La_2CuO_{4+\delta}$ undergoes a phase separation into domains that are rich or poor in interstitial oxygen, $O_i = O_\delta$.²⁰⁻²⁴ This is in contrast to homogeneous doping in the $La_{2-x}M_xCuO_4$ compounds. Superconductivity in $La_2CuO_{4+\delta}$ is granular, occurring in the O_i -rich domains, with only three discrete values of the transition temperature ($T_c = 17, 32, 42$ K) instead of a continuous superconducting T_c dome.^{24,25,28}

A structural analysis from neutron scattering²⁰ assigns interstitial oxygen in the O_i -rich domains to the $(\frac{1}{4}, \frac{1}{4}, -\frac{1}{6})$ positions between staggered LaO planes, called $O(4)$ (see Fig. 2). Occupying $O(4)$ positions between successive LaO double planes, interstitial oxygen ions align parallel to the crystal’s space diagonal, forming *commensurate* O_i^{2-} stripes of commensurability $(q_i^b, q_i^c)^{ortho} = (0.25, 0.5)$ in orthorhombic r.l.u.²²⁻²⁴

Residence of *ionized* excess oxygen at the $O(4)$ positions causes hole doping of the CuO_2 planes, where the holes reside pairwise in O atoms, as in $La_{2-x}Ae_xCuO_4$. Their magnetic moments, $\mathbf{m}(O) \neq 0$, give rise to magnetization stripes, as has been observed with neutron scattering.^{22,27} [Results from the two neutron investigations differ slightly, possibly as a result of different oxygen-enrichment procedures (electro-chemical, aqueous bath). Here we average the values from both investigations.] The magnetization stripes are oriented closely along the $Cu-O$ bonds (rotated off by $\sim 5^\circ$),^{22,27} with equal fractions along the tetragonal a^T and b^T axes.²⁸ Their incommensurability, converted to tetragonal r.l.u., is $q_m \simeq 0.115$. From the $q_c(x) = 2q_m(x)$ pattern of stripes in $La_{2-x}Ae_xCuO_4$, one would expect charge-order stripes in $La_2CuO_{4+\delta}$ parallel to the $Cu-O$ bonds, with $q_c \simeq 2 \times 0.115 = 0.23$. Instead, charge-order stripes of $q_c = 0.15$ are observed (converted to quasi-tetragonal r.l.u. from $q_c^{b,ortho} = 0.21$), *diagonal* to the $Cu-O$ bonds.^{21,24,26} How can that be understood?

In Ae -doped $La_{2-x}Ae_xCuO_4$, an incommensurability $q_m = 0.115$ results, by Eqs. (3, 1), from a hole density $p = x = 0.12$ in the CuO_2 planes. Since the same $q_m = 0.115$ is observed in oxygen-enriched $La_2CuO_{4+\delta}$, a hole density of $p = 0.12$ can also be assumed in that compound. The excess oxygen in $La_2CuO_{4+\delta}$ has been determined by gravitometry as $\delta = 0.12$.²² If all excess oxygen were embedded as O_i^{2-} ions at $O(4)$ sites, this would result in a hole density $p = 2\delta = 0.24$. The finding that magnetization stripes in $La_2CuO_{4+\delta}$ are caused by only *half* of the oxygen enrichment leaves open the possibility that the other half involves an embedding mechanism that is non-magnetic but modifies the charge order. We will return to this possibility in Sect. XII.

IV. CRYSTAL STRUCTURE AND DOPING

Before further comparison of stripes in $La_{2-x}Ae_xCuO_4$ and $YBa_2Cu_3O_{6+y}$, we need to get more familiar with the crystal structure of the compounds. Figure 2 shows a double unit cell of pristine La_2CuO_4 and a unit cell of $YBa_2Cu_3O_6$. The former crystal has the simpler structure, with LaO planes sandwiching the CuO_2 planes. However, its unit cells are vertically *staggered* with displacements by half the planar lattice constants, $(\frac{a_0}{2}, \frac{b_0}{2})$. Pristine La_2CuO_4 is orthorhombic with lattice constants $a_0 < b_0 < c_0$. Partial replacement of La^{3+} by the larger-sized $Ae^{2+} = Sr^{2+}, Ba^{2+}$ ions creates internal stress from lattice mismatch. The stress is relieved by a low-temperature phase transition to a tetragonal

structure, $a_0 = b_0 < c_0$, occurring near $x = 0.125$ when *Ba*-doped, but at $x = 0.21$ when *Sr*-doped.

In $YBa_2Cu_3O_6$, two CuO_2 planes sandwich the central *Y* plane. The CuO_2 -*Y*- CuO_2

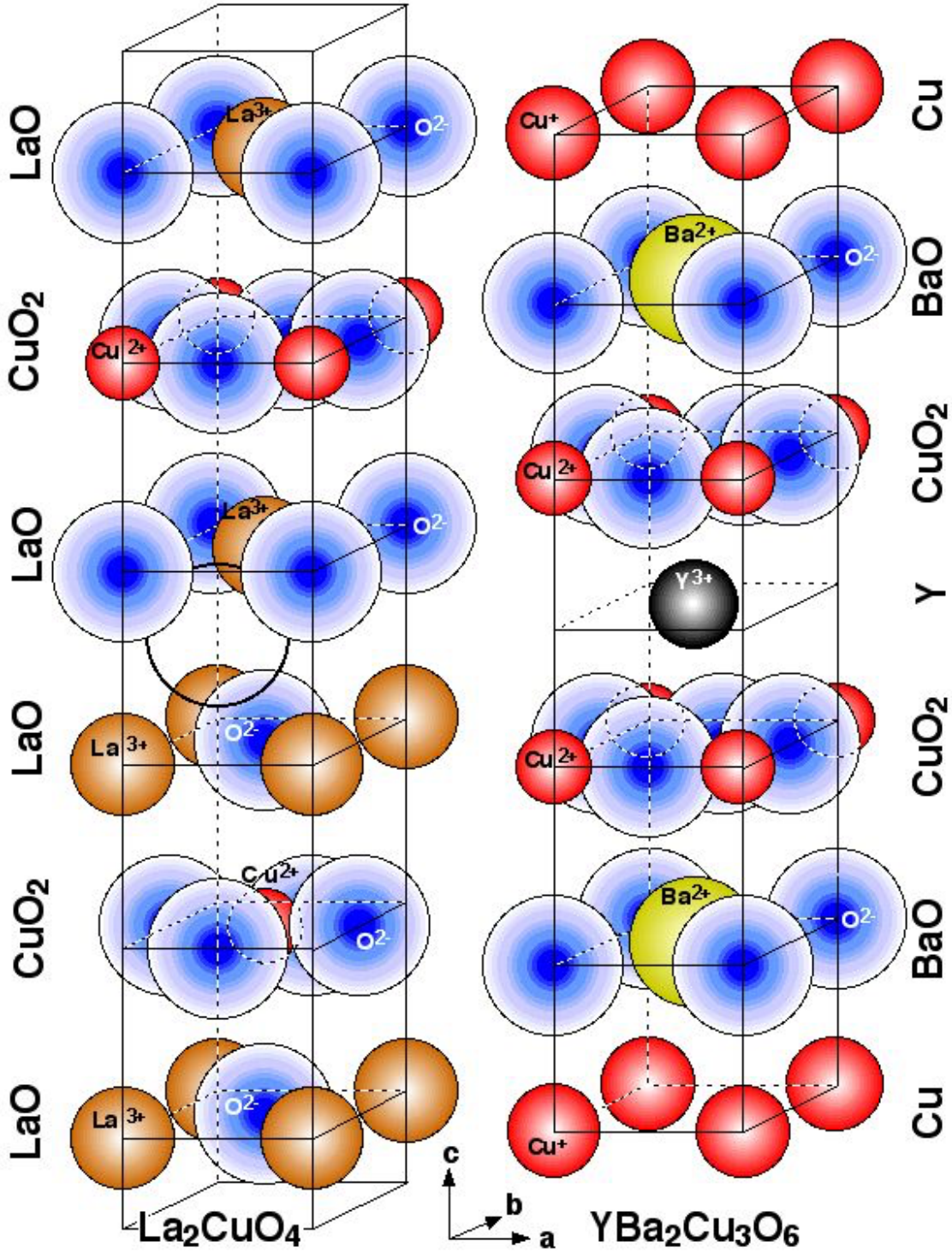
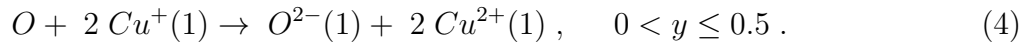


FIG. 2. Two unit cells of La_2CuO_4 (left) and single unit cell of $YBa_2Cu_3O_6$ (right), vertically exploded. Ion planes are noted on the sides. The black ring indicates an $O(4)$ site for an interstitial O^{2-} ion in La_2CuO_4 .

layer in turn is sandwiched by BaO - and terminal Cu -planes. Contrary to the ‘214’ compounds, $YBa_2Cu_3O_6$ is tetragonal but becomes orthorhombic upon oxygen doping at $y \approx 0.3$. Notice that by stoichiometry and charge balance, $Y^{3+}Ba_2^{2+}(Cu_2^{2+}Cu^+)O_6^{2-}$, the copper ions are in different ionization states, with Cu^{2+} ions in the CuO_2 planes but Cu^+ ions in the Cu planes (see Fig. 2). There are four possibilities how a doped oxygen atom can be embedded, labelled #1 to #4. For the sake of clarity they are introduced with the idealized assumption of a “0.5-watershed,” meaning that processes #1 and #2 occur only for oxygen doping $y \leq 0.5$ and processes #3 and #4 only for $y > 0.5$. The restriction, which captures most of the compound’s properties, will be relaxed later to account for some additional aspects.

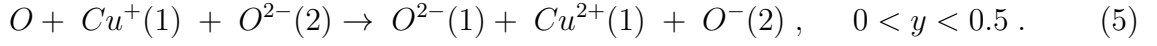
#1. A doped oxygen atom can be incorporated into the Cu plane between two Cu^+ ions, along the b -direction, contributing to a so-called CuO chain (see Fig. 3). In this case the oxygen atom takes two electrons from two neighboring copper ions in the Cu plane, denoted as $Cu^+(1)$. It results in higher ionization states of all three entities,



The $O(1) \rightarrow O^{2-}(1)$ embedding process can occur only for $y \leq 0.5$ but is exhausted at $y = 0.5$ when all former $Cu^+(1)$ ions have been ionized to $Cu^{2+}(1)$ ions. This can be seen by stoichiometry and charge balance of the resulting compound, $Y^{3+}Ba_2^{2+}Cu_3^{2+}O_{6.5}^{2-}$. It seems favorable, in terms of binding energy, that the doped oxygen aligns as $O^{2-}(1)$ ions in CuO chains. For $y = 0.5$ the configuration consists of alternate full and empty $O^{2-}(1)$ rows along the b -direction of the Cu planes, called “ortho-II oxygen ordered” (see Fig. 3). Note that process # 1 does not generate holes and thus *not* give rise to charge-order stripes in the CuO_2 planes.

#2. The second possibility of embedding is a variation of #1 that occurs as a result of imperfect crystal growth (here, insufficient annealing), but is absent in well-annealed crystals. Nevertheless, this (accidental) case provides some insight into stripe formation in $YBa_2Cu_3O_{6+y}$ and establishes a connection with stripes in the ‘214’ compounds, $La_{2-x}Ae_xCuO_4$. With increased filling of the CuO chains at oxygen doping $y < 0.5$, not every embedding O atom may find two close Cu^+ ions to take up two electrons. In this case it can take one electron from one nearby Cu^+ ion and “borrow” one electron from an oxygen ion in the CuO_2

plane, denoted as $O^{2-}(2)$, whose outer electron is less bound than in an $O^{2-}(2)$ ion of the intermediate BaO plane,¹



The process leaves temporarily an unstable $O^-(2)$ ion the CuO_2 plane, quickly to combine

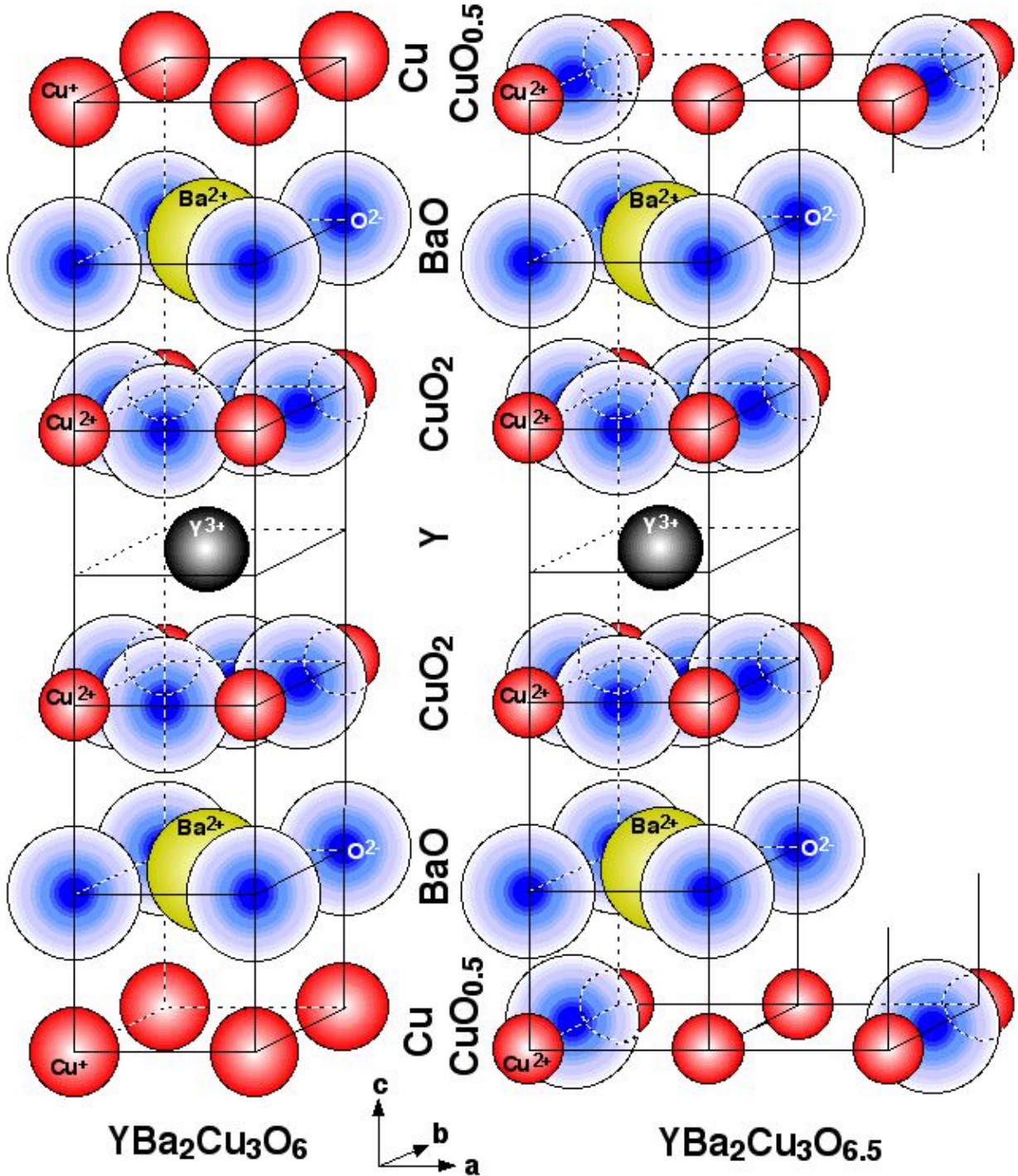


FIG. 3. Unit cell of $YBa_2Cu_3O_6$ (left) and of $YBa_2Cu_3O_{6.5}$ with ortho-II ordered CuO chains (right).

with another one to form a lattice-site oxygen *atom*,

$$2 O^-(2) \rightarrow O^{2-}(2) + O(2), \quad 0 < y < 0.5. \quad (6)$$

The assumption of unstable O^- ions is based on the experience with $La_{2-x}Ae_xCuO_4$, where doped holes reside pairwise in O atoms, instead of individually in O^- ions.¹ Coulomb repulsion spreads the double holes in under-annealed $YBa_2Cu_3O_{6+y}$, harbored by O atoms, to form an O superlattice. The resulting charge-order stripes then must have a square-root dependence on oxygen doping akin to Eq. (1), to be resumed shortly.

V. ANTIFERROMAGNETISM

The parent crystals La_2CuO_4 and $YBa_2Cu_3O_6$ are Mott insulators with antiferromagnetic order of the copper ions' magnetic moments, $\mathbf{m}(Cu^{2+})$, in the CuO_2 planes. Due to their closed electron shells, neither the oxygen ions contribute to magnetism, $\mathbf{m}(O^{2-}) = 0$, nor the copper ions in the $Cu(1)$ planes, $\mathbf{m}(Cu^+) = 0$. The stability of the parent crystals' 3D-AFM is dominated by the magnetic interaction between the CuO_2 planes. Because of orthogonal $\mathbf{m}(Cu^{2+})$ orientation in the widely separated, neighboring CuO_2 planes, compounded by the staggering of unit cells, 3D-AFM is relatively weak in La_2CuO_4 . It collapses when Ae -doped by $x_{N0} = 0.02$ —a very small Néel concentration. [This is the quantity that affects the offset value in Eq. (1), $\check{p} \leq x_{N0}$.] More Ae -doping, $x > x_{N0}$, leads to stripe formation in $La_{2-x}Ae_xCuO_4$, with incommensurability $q_{c,m}(x)$, as given by Eq. (1-3).

In $YBa_2Cu_3O_6$, by contrast, the CuO_2 planes that sandwich the central Y^{3+} planes are close and aligned, which gives rise to strong 3D-AFM. [The separation of neighboring $\mathbf{m}(Cu^{2+})$ moments along the c -direction is actually less than in the CuO_2 plane.] Oxygen doping by embedding process #1 generates additional $\mathbf{m}(Cu^{2+})$ moments in CuO chains along the b direction. They upset the 3D-AFM of the host and cause its collapse at $y_{N0} \simeq 0.30$ (but $0.25 < y_{N0} < 0.30$ when not well-annealed). With more oxygen doping, $y_{N0} < y < 0.5$, magnetization stripes are observed *only* if the crystal is insufficiently annealed, as mentioned. Their incommensurability rises from zero in a square-root dependence on doping (see Fig. 1). As noted, a square-root rise of the incommensurability is a signature of a superlattice of *defect charges*. In the present case the superlattice is formed by lattice-site O atoms in the CuO_2 planes, generated by process #2, carrying double holes. Their

magnetic moments, $\mathbf{m}(O)$, aligned in antiferromagnetic order, give rise to magnetization stripes, observed to be parallel to the crystal's a -axis. Taking into account that the unit cell of $YBa_2Cu_3O_{6+x}$ has *two* CuO_2 planes, the incommensurability of magnetization stripes depends on oxygen doping, akin to Eq. (1), as

$$q_m(y) = \frac{\sqrt{2}}{4} \sqrt{\frac{g}{2}(y - \check{y})}, \quad 0.25 < y < 0.50. \quad (7)$$

Here g is the fraction of doped oxygen atoms that are embedded by process #2. From the three known data points of magnetization stripes,²⁻⁵ the values of the offset \check{y} and the fraction g can be determined (see Appendix B). The result is $\check{y} = 0.27$, close to the collapse of 3D-AFM at $y_{N0} \approx 0.25$, and $g = 0.18$. The latter quantity means that between one-in-five and one-in-six doped oxygen atoms are embedded by the hole-generating process #2. Where are the charge-order stripes of double incommensurability that accompany the magnetization stripes? By analogy with doped lanthanum cuprates, $La_xAe_xCuO_4$, one can infer that they are, in this doping range, below the present detection limit.¹ The crystals where magnetization stripes have been observed, $0.30 \leq y \leq 0.45$, were annealed in the span of a day.²⁻⁵ However, such stripes are absent in crystals annealed over three months (and where $y_{N0} = 0.31$).⁶ This implies that the filling of CuO chains by “electron borrowing” from the CuO_2 planes (process #2) is a transitory phenomenon. But if the sample is cooled too fast, the attending magnetization stripes remain “frozen-in.”

VI. ORTHO-STRUCTURE OF OXYGEN CHAINS

Figure 1 shows that the magnetization stripes from incomplete annealing terminate when $y \rightarrow 0.5$. Oxygen doping of $YBa_2Cu_3O_{6+y}$ by embedding processes #1 or #2 is exhausted at $y = 0.5$. Larger oxygen doping, $y > 0.5$, affects both the $Cu(1)$ plane and each of the (two) adjacent CuO_2 planes,

$$y = \chi^{O(1)}(y) + 2\delta^{O(2)}(y). \quad (8)$$

The two contributions are determined by two processes, labelled #3 and #4, concerning oxygen embedding into CuO chains, $O(1)$, and respectively, into CuO_2 planes, $O(2)$.

#3. In the $Cu(1)$ plane, enriching oxygen *atoms*, O —instead of O^{2-} ions—now fill more than every other CuO chain. The chains—always along the b -direction—are called “ortho- N

oxygen ordered” when they have a periodicity Na in the a -direction.²⁹ The observed chain orderings are listed in Table I. The simplest cases are ortho-II with f-e sequence (full and empty chains alternating along the a -direction) and ortho-III with f-f-e sequence. The other orderings can be regarded as combinations thereof: V = II + III and VIII = III + II + III.

Although the doping fraction y can be accurately established by the proportion of ingredients to crystal growth, the *partition* of doped oxygen to the CuO chains and to the CuO_2 planes, Eq. (8), is not well known. Under the idealized assumption that the chains are completely full or empty—which is best approximated at prominent doping levels \underline{y} —along with the “0.5-watershed,” we can use the perfect fill ratio, $\phi_\infty^{O(1)} = N_f/N$, where N_f is the number of full chains in an ortho-N oxygen order. With $\chi^{O(1)}(\underline{y}) \approx \phi_\infty^{O(1)}(\underline{y})$, Eq. (8) gives

$$\delta_{0.5}^\infty(\underline{y}) \approx \frac{\underline{y} - \phi_\infty^{O(1)}(\underline{y})}{2}, \quad (9)$$

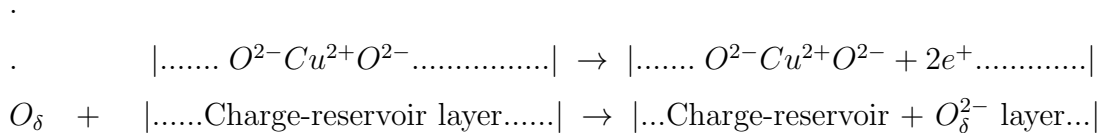
listed in Table I. At $y = 0.5$, the $Cu(1)$ plane is almost perfectly covered by ortho-II CuO chains, as attested by very high correlation lengths, $\xi_b(\underline{y})/b_0 = 112$ and $\xi_a(\underline{y})/a_0 = 39$.³⁰ Other cases of CuO chains, while long, are not completely filled, as indicated by the observed chain-order correlation length $\xi_b(\underline{y})/b_0$ in Table I. Nevertheless, the $\delta_{0.5}^\infty(\underline{y})$ values in the table give a rough estimate and overview of the density of oxygen atoms in the CuO_2 planes.

oxygen content	prominent \underline{y}	chain ortho-N	chain sequence	$\phi_\infty^{O(1)}(\underline{y})$ in the $Cu(1)$ plane	$\delta_{0.5}^\infty(\underline{y})$ in each CuO_2 plane	$\xi_b(x)/b_0$ chains	$\xi_\tau(y)/\tau_0$ stripes
$0.35 \leq y \leq 0.50$		II =	f-e (spotty)			44	10
$0.50 < y \leq 0.6$	1/2	II =	f-e	1/2 = 0.50	0.00	61	17
$y = 0.62$		(II&) V =	f-e-f-f-e	3/5 = 0.60	0.01		
$y \simeq 0.67$	2/3	VIII =	f-f-e-f-e-f-f-e	5/8 = 0.625	0.02	36	26
$0.72 \leq y \leq 0.82$	3/4	III =	f-f-e	2/3 = 0.667	0.04	30	11

TABLE I: CuO chains in the $Cu(1)$ planes of $YBa_2Cu_3O_{6+y}$ with ortho-N ordering along the a -direction of full (f) and empty (e) chains along the b -direction at prominent doping levels \underline{y} . The quantity $\phi_\infty^{O(1)} = N_f/N$ is perfect fill ratio and $\delta_{0.5}^\infty(\underline{y})$, Eq. (9), is the density of O atoms embedded in each CuO_2 plane at prominent doping levels \underline{y} , based on idealized assumptions. The observed correlation lengths (Refs. 8-11, 14, 15) are denoted by ξ , with b -axis lattice constant b_0 and $\tau = a, b$.

VII. CONVENTIONAL VIEW OF HOLE DOPING BY OXYGEN ENRICHMENT

Charge-order stripes are observed in the CuO_2 planes of $YBa_2Cu_3O_{6+y}$ for oxygen doping $y > 0.5$. (Exceeding the assumption of the “0.5-watershed,” weak stripes appear already in the $0.45 < y < 0.5$ interval). The part of oxygen doping that is not consumed by CuO chain filling, but causes charge-order stripes in each CuO_2 plane, is denoted as $\delta(y)$, Eq. (8). *Common wisdom* has it, that each stripe-forming oxygen atom, O_δ , upon taking two electrons from an O^{2-} ion in an CuO_2 plane, resides as an interstitial ion, O_δ^{2-} , in the so-called charge-reservoir layer (which comprises all planes of the unit cell other than CuO_2). This amounts to hole doping of the CuO_2 plane:



If, like in $La_{2-x}Ae_xCuO_4$, the doped holes react as $2e^+ + O^{2-} \rightarrow O$ to form lattice-site O atoms, their superlattice would give rise to charge-order and magnetization stripes with a square-root dependence of $q_{c,m}(\delta)$, akin to Eqs. (1, 3). However, *no such stripes are observed* in $YBa_2Cu_3O_{6+y}$ (for $y > 0.5$), but $q_c(\delta) \approx 0.3$ and *no* magnetization stripes at all (see Fig. 1). Therefore, the conventional view cannot be correct.

VIII. OXYGEN EMBEDDING IN THE CuO_2 PLANES

Concerning the implementation of stripe-forming oxygen for $y > 0.5$, five observations shall be pointed out, all visible in Fig. 1: (i) the onset of charge-order stripes with a *non-zero* value, $q_c^{ons} \neq 0$; (ii) the stripes’ incommensurability $q_c(y)$ *not* having a rising square-root dependence; (iii) the near *constancy* of $q_c(y)$, *decreasing* slightly at larger y ; (iv) the specific range of $q_c(y) \simeq 0.3$ r.l.u., and (v) the *lack* of accompanying magnetization stripes. The five observations give rise to five implications: (i) The non-zero onset suggests a *different* mechanism of stripe formation than of the magnetization stripes at $y \approx 0.25$ with $q_m^{ons} = 0$ (and as known from $q_{c,m}^{ons} = 0$ of the ‘214’ compounds). (ii) The absence of a rising square-root dependence of $q_c(y)$ indicates that these stripes are *not* formed by entities with lattice-defect charges, like double holes in lattice-site O atoms, that would spread by Coulomb repulsion. (iii) Leaving the slight y -dependence of $q_c(y)$ aside (until Sect. IX), a *constant* incommensu-

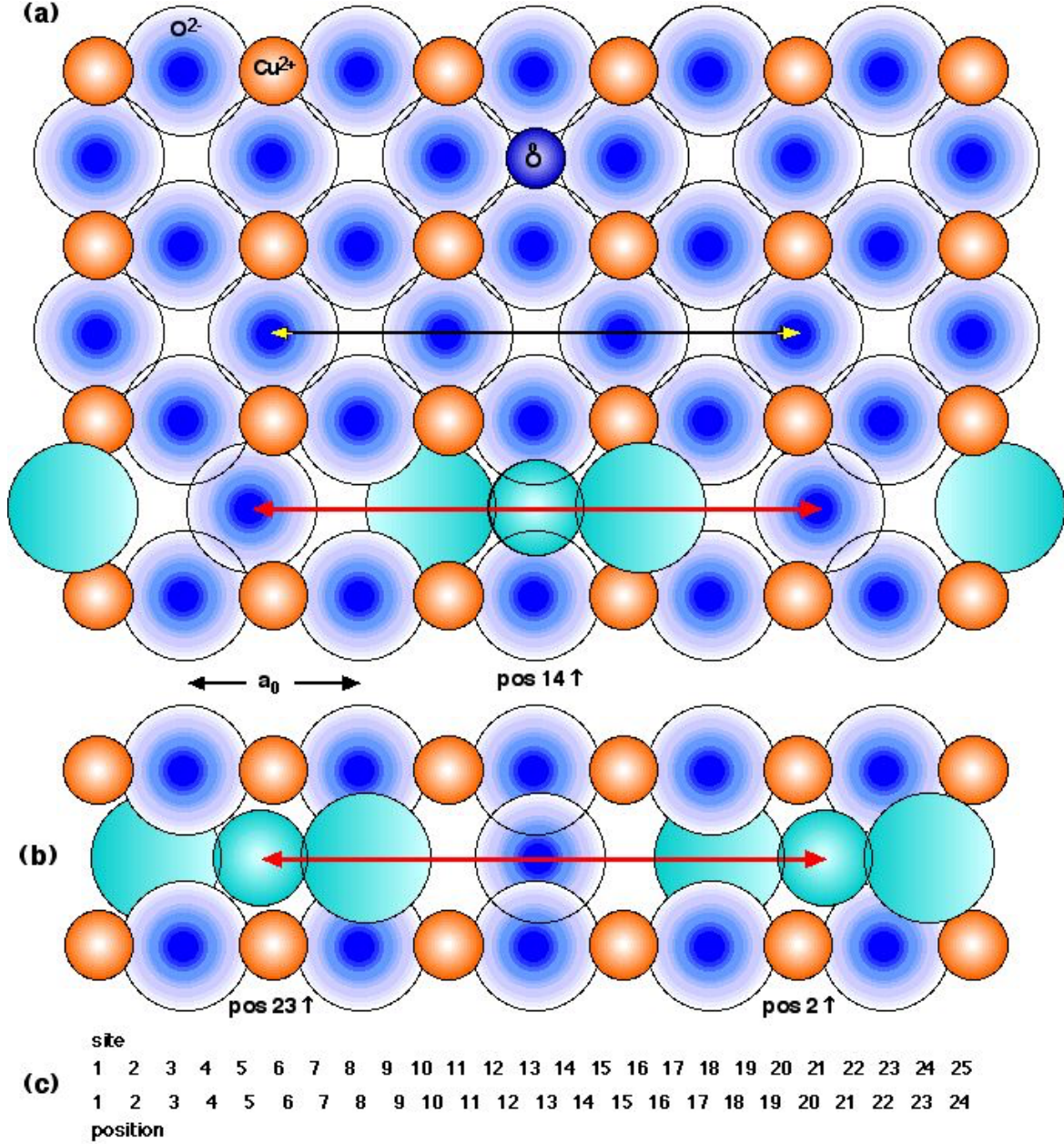
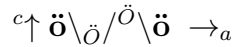


FIG. 4. (a) Excess oxygen in the CuO_2 plane of $YBa_2Cu_3O_{6+y}$ ($y \simeq 0.55$), shown schematically for an oxygen atom at the stages of embedding (second row) and final relaxation (sixth row). In the space (“pore”) between four O^{2-} ions (denoted for short as \ddot{O}), the embedded oxygen atom (denoted as \ddot{O}) bonds with two O^{2-} neighbors, here in the a -direction, to form an ozone molecule ion, $\ddot{O}\ddot{O}\ddot{O}$ (turquoise color). Each $\ddot{O}\ddot{O}\ddot{O}$ motif of three internuclear distances occupies a length of $3.125 a_0$ (red double arrow), slightly larger than $3a_0$ (black double arrow). Thus a train of eight contiguous $\ddot{O}\ddot{O}\ddot{O}$ motifs would spread over $25a_0$. The $\ddot{O}\ddot{O}\ddot{O}$ and \ddot{O} positions in row 6 are (approximately) relaxed, but the Cu^{2+} and O^{2-} ions in row 5 and 7 are shown (for comparison) at non-relaxed sites. (b) Different part of the $\ddot{O}\ddot{O}\ddot{O}$ train, with the middle row relaxed but the row above and beneath non-relaxed. (c) Scheme of ideal lattice sites and $\ddot{O}\ddot{O}\ddot{O}$ positions.

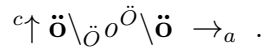
as assistance of parallel spins in reducing Coulomb repulsion between the O atom's lone p orbitals. In the $\ddot{O}\ddot{O}\ddot{O}$ molecule, by contrast, the lone p orbitals, located about the terminal nuclei, are far apart. Thus no assistance from parallel spins is necessary to reduce their much smaller Coulomb repulsion. Instead, it is energetically favorable that the lone p orbitals profit in energy from magnetic attraction of antiparallel spins.

Besides the arguments based on stripe incommensurability—non-zero onset, no square-root dependence, nearly constant $q_c(y) \approx 0.3$, no magnetization stripes—is there other experimental support for the proposed stripe formation in $YBa_2Cu_3O_{6+y}$ ($y > 0.5$) by interstitial oxygen, $\overset{\circ}{O}$, in the CuO_2 planes? A hard-X-ray investigation of ion displacements in $YBa_2Cu_3O_{6.54}$, evaluated from intensities of *all* available charge-order satellite peaks, showed an accordion-like, incommensurate folding of the CuO_2 planes, with distinct out-of-plane displacements.¹⁷ For example, for stripes along the a -direction, the four $O^{2-} = \ddot{O}$ ions at positions $(0, \frac{1}{2}, 0)$, $(1, \frac{1}{2}, -c)$, $(2, \frac{1}{2}, +c)$, $(3, \frac{1}{2}, 0)$ —as in row 4 of Fig. 4(a)—look like



in the $(a, \frac{1}{2}, c)$ plane, spanned by the axial arrows. The bold \ddot{O} ions are in the CuO_2 plane ($c = 0$), and the $\mp c$ -displacements of the middle \ddot{O} ions are exaggerated. The folding pattern is continued periodically along a .

What would compel the host CuO_2 planes, upon oxygen doping $y > 0.5$, to fold like this? As a common experience, a thin piece of material—say a ribbon or a foil—folds when enlarged while being confined to one or two dimensions, by extending in a perpendicular dimension. This basic phenomenon may also be exhibited by the CuO_2 planes of $YBa_2Cu_3O_{6+y}$. The corresponding “enlargement” may well be caused by interstitial $\overset{\circ}{O}$ atoms that bond with neighboring O^{2-} ions to form ozone ions, $\ddot{O}\overset{\circ}{O}\ddot{O}$. Space constraints along the stripes' direction, here along a , make these ions tilt, causing a folding pattern like



The interstitial $\overset{\circ}{O}$ atom is at the pore position, $(\frac{3}{2}, \frac{1}{2}, 0)$, like in row 2 of Fig 4(a). (Graphical constraints prohibit the over-ring to be shown in the last folding pattern.) Qualitatively, the similarity of \ddot{O} ion displacements in both folding patterns is striking. While the reason for folding the host CuO_2 plane (without $\overset{\circ}{O}$, top pattern) is not obvious, space requirement makes it necessary when $\overset{\circ}{O}$ is present (bottom pattern).

Getting back to the top folding pattern of host ion displacements, obtained from the X-ray investigation, not only do the O^{2-} ions in the $(a, \frac{1}{2}, c)$ plane [row 4 in Fig. 4(a)] have large $\mp c$ displacements, but also their neighbors in the CuO_2 plane [rows 3 and 5 in Fig. 4(a)]. The next diagram shows these neighbors, displayed in the corresponding $(a, \frac{1}{2} \mp \frac{1}{2}, c)$ planes that bracket the central $(a, \frac{1}{2}, c)$ plane. (The middle line, labelled ‘ $b = \frac{1}{2}$,’ is a repetition of the top folding pattern above.) The bracketing $(a, \frac{1}{2} \mp \frac{1}{2}, c)$ planes contain both $Cu^{2+} \equiv \ddot{C}$ and $O^{2-} \equiv \ddot{O}$ ions, with separation $\ddot{C}-\ddot{O} = a_0/2$ in the a -direction [see rows 3 and 5 in Fig. 4(a)]. For the sake of clarity, the $Cu^{2+} = \ddot{C}$ and $O^{2-} = \ddot{O}$ ions are displayed separately (top and bottom line of the following diagram, labelled ‘ $b = 0, 1$,’), with the understanding that the ions of *both* lines bracket the center line on both sides [as in rows 3 and 5 of Fig. 4(a)].



Now we can also see out-of-plane \pm displacements of the middle \ddot{C} and terminal \ddot{O} ions in the $b = 0, 1$ lines: They are opposite to the $\mp c$ displacements of the middle \ddot{O} ions in the $b = \frac{1}{2}$ line—with a “butterfly pattern of oxygen shear displacements”¹⁷—as if they want to avoid each other. Why?

The pattern of host ion displacement makes sense when we insert an interstitial $\overset{\circ}{O}$ atom in the central line, $b = \frac{1}{2}$, shown in the next folding pattern. Space constraints along the a -direction causes the ensuing ozone ion, $\overset{\circ}{O}\ddot{O}\overset{\circ}{O}$, to tilt out of the CuO_2 plane. The neighbor ions in the $b = 0, 1$ lines accommodate the tilt by getting out of the way.



As a technical note, charge-order stripes in the b -direction of in $YBa_2Cu_3O_{6.54}$ are much more prevalent than along a (see Sect. IX). Consequently, the X-ray evaluation of host-ion displacements is much more accurate for b -stripes than for a -stripes. The present explanation of out-of-plane folding for a -stripes was done for ease of display. All conclusion hold equally for b -stripes.

The X-ray investigation of host-ion displacements¹⁷ showed no direct evidence of excess oxygen in the CuO_2 planes. Subject to symmetries and certain constraints, the evaluation

of the diffraction intensities was based on the best fit of all displacements of all host ions in the unit cell. Mirror symmetry with respect to the $Cu(1)$ planes was assumed and group-theoretical constraints were invoked. However, no allowance for interstitial oxygen in the CuO_2 planes was provided in the evaluation—thus none *could* be found. Nevertheless, the host-ion displacements from the investigation are, on a qualitative level, compatible with the presence of interstitial oxygen in the CuO_2 planes and the observed folding is compatible with out-of-plane tilts of $\ddot{O}\ddot{O}\ddot{O}$ ions. It would be desirable to reevaluate the X-ray intensities¹⁷ with allowance for interstitial oxygen in the CuO_2 planes.

IX. INCOMMENSURABILITY AND AXIAL PREFERENCE OF STRIPES

In order to go beyond the simplified assumption of constant incommensurability, treated in the previous section, three observations must be taken into account. (i) Figure 1 shows that the q_c data decrease by 13% from $q_c^b(0.45) = 0.33 = \frac{8}{24}$ to $q_c^a(0.90) = 0.29 = \frac{8}{28}$. This means that the $\ddot{O}\ddot{O}\ddot{O}\ddot{O}$ length increases such that a train of eight contiguous $\ddot{O}\ddot{O}\ddot{O}\ddot{O}$ motifs extends with increasing y over a distance from 24 to 28 lattice sites, respectively. (ii) Figure 1 also shows that for a given oxygen doping y , stripe incommensurability along the b -axis is always larger than for stripes along the a -axis, $2(q_c^b - q_c^a)/(q_c^b + q_c^a) \approx 3\%$. (iii) At $y \approx 0.55$, the peak intensity of X-rays diffracted by charge-order stripes is dominant for stripes along the b -direction, but very weak for stripes along a .¹⁴ (The intensity of stripes is not indicated in Fig. 1.) At $y = 0.67$, peak intensities are about equal for stripes along b and a .¹⁴ With $y > 0.67$, the peak intensity gets increasingly stronger for a -stripes but weaker for b -stripes.¹⁴ This means, there is an axial preference of the stripes, depending on oxygen doping. The three observations raise three questions: (i) Why does $\bar{q}_c(y)$ decrease with increasing doping? (ii) Why is always $q_c^b(y) > q_c^a(y)$? (iii) What is the reason for the change of axial preference with increasing oxygen doping?

From the incommensurability $q_c^b = 0.33$ of the very weak stripe signal, measured at $y = 0.45$, we can infer that an *isolated* $\ddot{O}\ddot{O}\ddot{O}\ddot{O}$ motif, with its tilted central ozone ion, projects on the b -axis to a length $L^b = b_0/q_c^b = 3b_0$. When, with increasing oxygen doping, several $\ddot{O}\ddot{O}\ddot{O}\ddot{O}$ motifs axially connect, van-der-Waals attraction—specifically between their out-of-plane \ddot{O} members (marked bold in the diagram)—reduce the ozone tilt,

$$c\uparrow \ddot{o}\ddot{o}o\ddot{O}\ddot{o}\ddot{o}o\ddot{O}\ddot{o} \rightarrow_{a,b} ,$$

with subsequent increase of their projected axial length, $\bar{L}(y)$. This explains, qualitatively, the slight decrease of incommensurability with oxygen enrichment, $\bar{q}_c(y) = s_0/\bar{L}(y)$.

For a quantitative assessment, we relax the idealized assumption of the “0.5-watershed” which served in introducing oxygen-implementation separately for processes #1,2 and #3,4. Experimental evidence from the onset of stripes and of superconductivity indicates that to a small degree processes #4 commences already at $y < 0.5$. Accordingly, process #1 extends in the same (small) degree to $y > 0.5$. Motivated by the quest for a common description for *all* (*Y*-, *Hg*-, *Bi*-based) oxygen-enriched cuprates, we express the dependence of stripe incommensurability on the density δ of excess oxygen in each CuO_2 plane empirically as

$$\bar{q}_c(\delta) = \bar{q}_c(y_c^{ons}) - \gamma \times [\delta(y) - \delta(y_c^{ons})] . \quad (11)$$

Here the superscript ‘*ons*’ indicates the onset of charge-order (*c*) stripes. The onset incommensurability, $\bar{q}_c(y_c^{ons})$, is material-specific, typically in the range $0.33 > \bar{q}_c(y_c^{ons}) > 0.26$. Both the coefficient $\gamma \simeq 0.67/\text{r.l.u.}$ and the onset density $\delta(y_c^{ons}) \simeq 0.04$ (evaluated in Sect. X) hold for the whole *family* of oxygen-enriched cuprates. Values of δ , calculated with Eq. (11) and $\bar{q}_c(y)$ data from experiment, are listed in Table II. Their increase over the onset, $\delta - \delta(y_c^{ons}) = \delta - 0.04 \simeq \delta_{0.5}^\infty$, is comparable with the density of excess oxygen in the CuO_2 plane obtained with idealized assumptions (“0.5-watershed,” filled CuO chains, Table I).

Turning to the second question—why is $q_c^b(y) > q_c^a(y)$?—one third of the 3% difference of $q_c^{b,a}$, that is 1%, is a consequence of orthorhombic anisotropy: The same actual length of

y	\bar{q}_c expt.	$\delta_{0.5}^\infty \leftarrow$ Table I	$\delta \leftarrow$ Eq. (11)	$p \leftarrow$ Universal Dome	Comment
0.31(1)				0.05	Onset of superconductivity
0.45	0.323		0.04	0.08	Onset of charge stripes
0.67	0.308	0.02	0.06	0.12	Maximal stripe intensity
0.75	0.303	0.04	0.07	0.14	Ignoring the dip of $T_c(y)$
0.92	0.297		0.08	0.16	$T_{c,max} = 93.5$ K

TABLE II: Density $\delta(y)$ of stripe-forming oxygen in the CuO_2 planes of $YBa_2Cu_3O_{6+y}$, calculated with Eq. (11) and $\bar{q}_c(\delta)$ data from experiment. The δ values exceed the onset value, $\delta = 0.04$, by about $\delta_{0.5}^\infty$ from Table I, obtained with idealized assumptions. The hole density p is obtained with the universal-dome method (discussed in Sect. XIII).

an $\ddot{O}\ddot{O}\ddot{O}$ motif (at a given y value) appears 1% smaller when expressed in terms of the lattice constant b_0 than of a_0 because of $2(b_0 - a_0)/(b_0 + a_0) \approx 1\%$. The remaining 2% difference (at the same y value) is caused by the presence or absence of *squeeze* from full or, respectively, empty CuO chains in the $Cu(1)$ plane onto the tilted ozone ions in the CuO_2 planes. This can be seen in Fig. 5, which holds for oxygen doping $y \simeq 0.55$, when the CuO chains along b are ortho-II oxygen ordered (alternately full and empty). Along the a -direc-

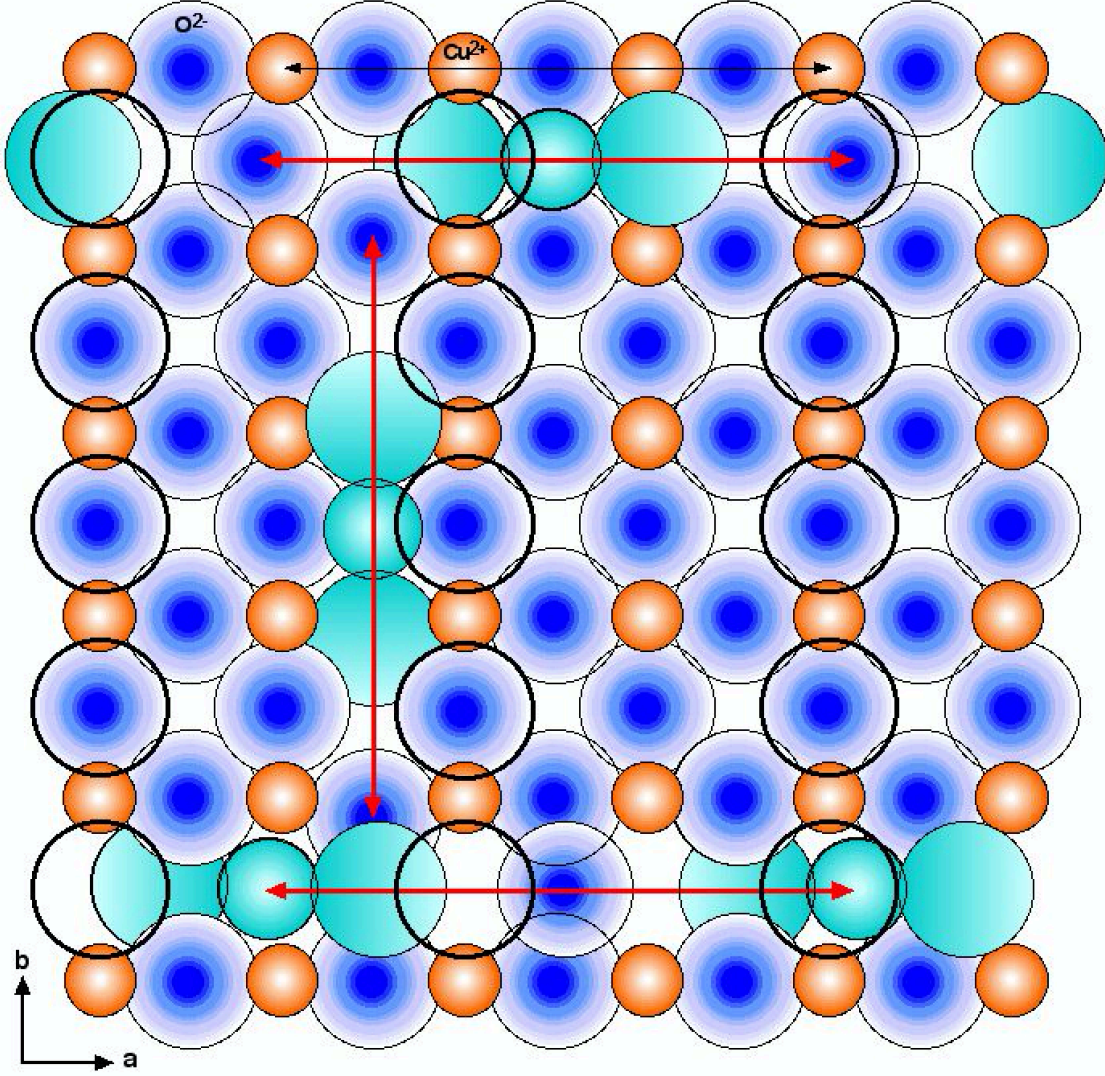


FIG. 5. Depression of the tilt of ozone ions $\ddot{O}\ddot{O}\ddot{O}$ (turquoise) by CuO chains (heavy rings), here in ortho-II order ($y \simeq 0.55$): Central squeeze by full CuO chains reduces the tilt of $\ddot{O}\ddot{O}\ddot{O}_a$ ions along a . This increases the projected length, L^a (horizontal red arrows), of $\ddot{O}\ddot{O}\ddot{O}_a$ motifs. In contrast, the $\ddot{O}\ddot{O}\ddot{O}_b$ ions along b are squeezed by CuO chains only on one side, causing less tilt depression (sideway evasion), such that $L^b < L^a$ and $q_c^b(y) > q_c^a(y)$. At higher doping, less empty CuO chains are available. Rather than being squeezed from full CuO chains on both sides (not shown), $\ddot{O}\ddot{O}\ddot{O}$ ions then prefer to align along a , instead of b .

tion, the tilt of the ozone ions is depressed by the O^{2-} ions in the CuO chains above (or below)—shown by heavy circles—causing a longer projected length L^a of the $\ddot{O}\ddot{O}\ddot{O}$ motifs. Figure 5 also shows that, with ortho-II oxygen ordering, tilted ozone ions along the b -directions are squeezed by a full CuO chain only on *one side* but not by the empty CuO chain on their other side. Shifting sideways, b -oriented $\ddot{O}\ddot{O}\ddot{O}$ ions can partly evade the squeeze, resulting in $L^b < L^a$. This explains, qualitatively, $q_c^b(y) > q_c^a(y)$.

Turning to the question of axial preference, one-sided depression of tilted ozone ions along b seems to be energetically preferable to central depression of $\ddot{O}\ddot{O}\ddot{O}$ ions along a by full CuO

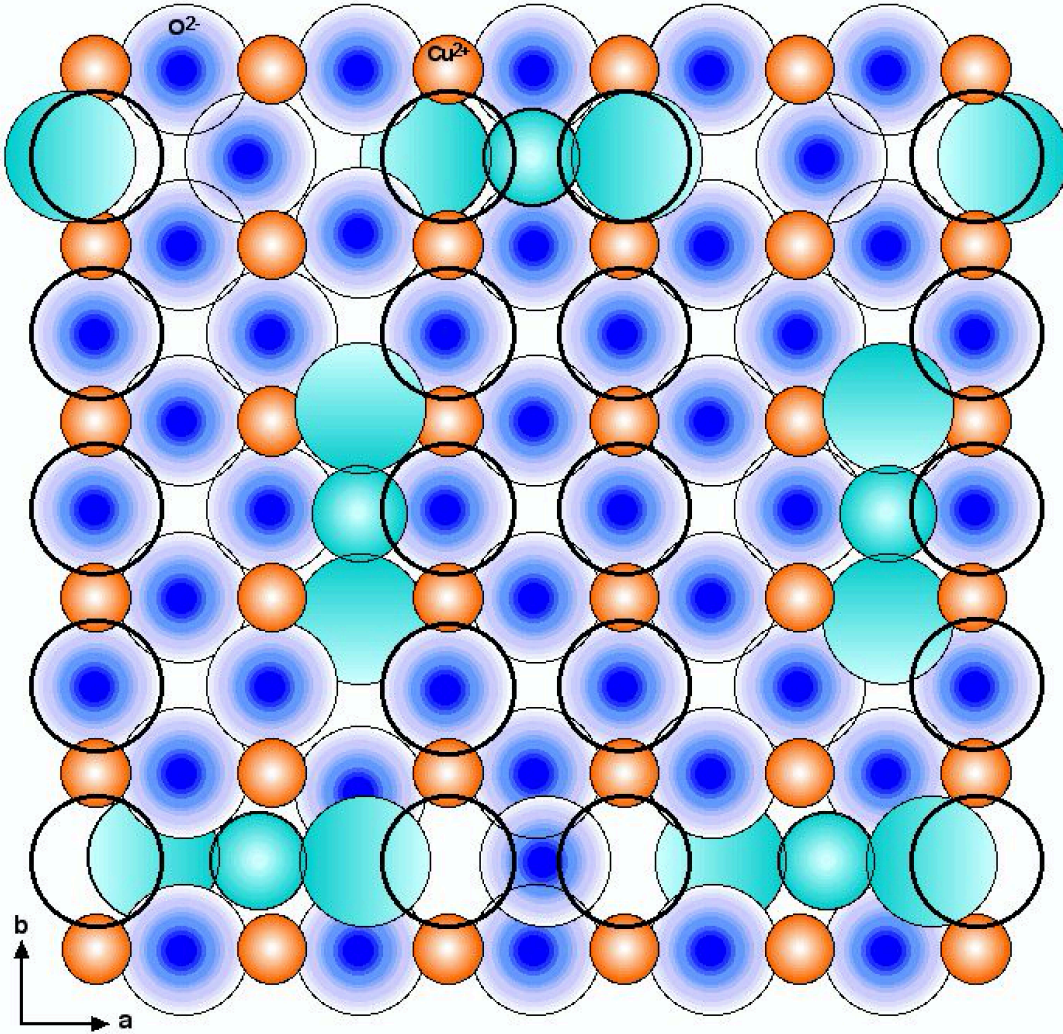


FIG. 6. CuO_2 plane of $YBa_2Cu_3O_{6.67}$ with ortho-VIII oxygen order (ffeffeffe) and ozone ions. When compressed along a , CuO chains (black rings) transmit the increased tilts of $\ddot{O}\ddot{O}\ddot{O}_a$ ions to the next CuO_2 plane where some ozone ions rotate, $\ddot{O}\ddot{O}\ddot{O}_{a \rightarrow b}$. But when compressed along b , no increased tilt of $\ddot{O}\ddot{O}\ddot{O}_b$ ions is translated, as the CuO chains unilaterally slide by. This causes the asymmetry of 3D stripe order: Increase of 3D b -stripes when compressed along a , but no change of 3D a -stripes when compressed along b .

chains. This would explain the prevalence of b -stripes in the range $0.45 < y < 0.6$. What happens at denser ortho-N oxygen structures, for $y > 0.6$, when every other CuO chain is no longer empty? Depression of b -oriented ozone ions along b on *both* sides by full CuO chains seems to be prohibitive. Thus, when less empty CuO chains are available at higher doping, the ozone ions rather align along a , instead of b . This explains, qualitatively, the shift of the stripes' axial preference from the b -direction to the a -direction at high oxygen doping.

How long are the trains of $\ddot{O}\ddot{O}\ddot{O}$ motifs? Guided by correlation lengths $\xi_c^{a,b}(y)$ (Tab. I) the trains are ~ 3 motifs long, $\ddot{o}_{\ddot{O}}o\ddot{O}\ddot{o}_{\ddot{O}}o\ddot{O}\ddot{o}_{\ddot{O}}o\ddot{O}$ at $y = 0.5$;
 rising to a maximum of ~ 6 motifs, $\ddot{o}_{\ddot{O}}o\ddot{O}\ddot{o}_{\ddot{O}}o\ddot{O}\ddot{o}_{\ddot{O}}o\ddot{O}\ddot{o}_{\ddot{O}}o\ddot{O}\ddot{o}_{\ddot{O}}o\ddot{O}\ddot{o}_{\ddot{O}}o\ddot{O}$ at $y = 0.67$;
 and steadily decrease to ~ 2 motifs, $\ddot{o}_{\ddot{O}}o\ddot{O}\ddot{o}_{\ddot{O}}o\ddot{O}$ at $y = 0.9$.

Very recently, charge-order stripes have been investigated with RIXS for $YBa_2Cu_3O_{6.67}$ (where the $\ddot{O}\ddot{O}\ddot{O}$ trains are longest and about equally oriented along a and b), subject to uniaxial compression.³¹ It was found that (i) compression in the a -direction increases the intensity, and decreases the peak width, of the RIXS signal from 2D stripes (that is, in the CuO_2 planes) along the b -direction, and vice-versa. (ii) Compression in the a -direction also increases 3D stripe order along b , but compression along b leaves 3D stripe order along a unchanged.

The first finding is readily explained with the present model: Ozone ions avoid constraint in the compressed direction by populating the orthogonal direction. The asymmetry of the second finding is a consequence of the directional asymmetry of the CuO chains: Extending along b , the CuO chains transmit increased $\ddot{O}\ddot{O}\ddot{O}$ tilts from one CuO_2 plane to the next *differently* for compression along a or b , as illustrated in Fig. 6.

X. STRIPES IN $HgBa_2CuO_{4+\delta}$

Mercury-based $HgBa_2CuO_4$ has a tetragonal lattice.^{32,33} Its unit cell has one CuO_2 plane at the center, sandwiched by BaO layers, and terminated with planes of Hg^{2+} ions at the top and bottom (see Fig. 7). When the compound is enriched with oxygen, $HgBa_2CuO_{4+\delta}$, it becomes superconducting, with $T_{c,max} = 98$ K.³² Where will the excess oxygen atoms be embedded? The conventional assignment, based on neutron scattering^{32,33} and X-ray diffraction,³⁴ is at the center of the Hg planes, $(\frac{1}{2}, \frac{1}{2}, \frac{1}{2} \pm \frac{1}{2})$, called the $O(3)$ position. Evidence for the $O(3)$ position is indirect: (i) It is supported by Rietveld refinement of the scattering

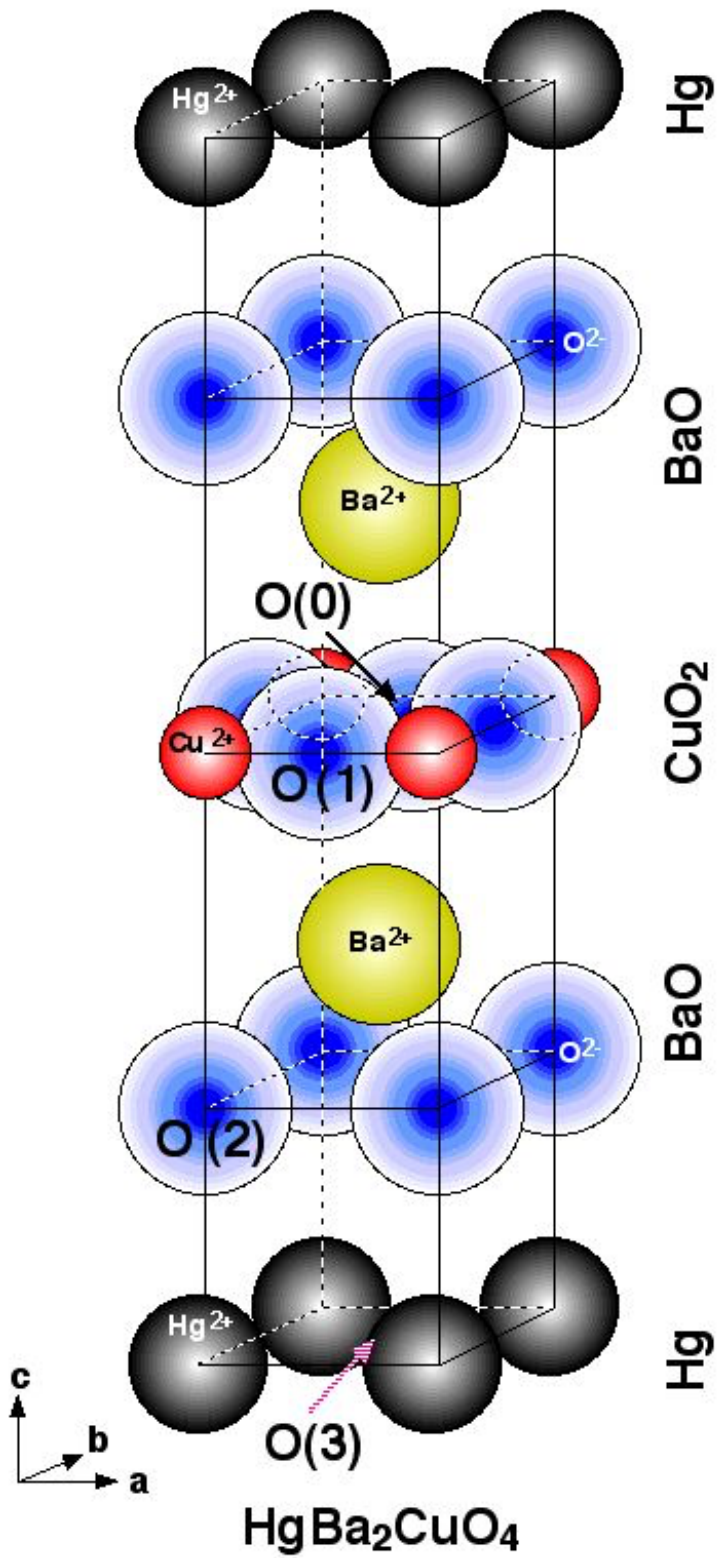


FIG. 7. Unit cell of $HgBa_2CuO_4$ in hard-sphere display, vertically exploded. Ion planes and layers are noted on the side. Crystallographic notation of lattice site oxygen, $O(1)$ and $O(2)$, is given, and of hypothetical sites for interstitial oxygen, $O(3)$ and $O(0)$.

data.^{32–34} (ii) The decreasing separation of the Ba and $O(2)$ planes with oxygen enrichment is interpreted as the result of charge-transfer from $O(3)$ sites to the CuO_2 planes.³²

Deviating from the conventional assignment, it is assumed here that excess O atoms are embedded in the center of CuO_4 plaquettes—the “pores”—as in $YBa_2Cu_3O_{6+y}$, here at the $O(0) \equiv (\frac{1}{2}, \frac{1}{2}, \frac{1}{2})$ position. The deviation is motivated by the quest for a common embedding mechanism of excess oxygen O_δ in the CuO_2 planes of *all* (Y -, Hg -, Bi -based) oxygen-enriched high- T_c cuprates. Supporting arguments for the deviation are: (i) The $O(0)$ position for O_δ was never probed in the Rietveld refinement of scattering data.^{32–34} (ii) Although there is ample space for an O atom at the $O(3)$ position between the four Hg^{2+} ions, there is little incentive for it in terms of chemical bonding. However, a gain of cohesive energy would occur at $O(0)$ through formation of an ozone ion, $\ddot{O}\ddot{O}\ddot{O}$, from the excess O_δ atom with two axial O^{2-} neighbors. (iii) Neutron scattering experiments show that the $Ba-O(1)$ and $Hg-O(2)$ bonds are essentially rigid, but that the $Cu-O(2)$ and $Ba-O(3)$ distances change considerably with pressure.³³ Due to the rigid $Ba-O(1)$ and $Hg-O(2)$ layers, compression of the crystal then results in a lesser separation of the Ba and $O(2)$ planes. Accordingly, the observed approach of the Ba and $O(2)$ planes upon enrichment³² can be interpreted to result from internal pressure exerted by excess O_δ , located at *either* the $O(3)$ *or* $O(0)$ position. If O_δ resides at $O(3)$, then one would expect that the $Hg-O(3)$ distance becomes rigid at higher δ . It is observed, however, that the pressure dependence of the $Hg-O(3)$ distance is independent of oxygen enrichment.³³ Combined with the compressibility of all bonds, the finding is in favor of O_δ residence at $O(0)$ instead of $O(3)$ sites.

Charge-order stripes appear in $HgBa_2CuO_{4+\delta}$ at oxygen enrichment $\delta_c^{ons} = 0.037$ with incommensurability $q_c^{ons} = 0.292$ when the transition temperature to superconductivity is $T_c(\delta^{ons}) = 55$ K, and disappear at $\delta_c^{fin} = 0.085$ with $q_c^{fin} = 0.260$ when $T_c(\delta^{fin}) = 88$ K (Refs. 33, 35). Assuming that all enriching oxygen is embedded in the CuO_2 planes permits a determination of the family-specific rate for stripes in oxygen-enriched CuO_2 planes,

$$\gamma = \frac{q_c^{fin} - q_c^{ons}}{\delta^{fin} - \delta^{ons}} = \frac{0.292 - 0.260}{0.085 - 0.037} = 0.67. \quad (12)$$

Inserting the value into Eq. (11) gives a formula for the dependence of stripe incommensurability on oxygen enrichment of $HgBa_2CuO_{4+\delta}$,

$$q_c(\delta|HgBa_2CuO_{4+\delta}) = 0.292 - 0.67(\delta - 0.037). \quad (13)$$

From the observed correlation length of the stripes,³⁵ $\xi \approx 7.5a_0$, one can infer that the stripes consist of trains of two motifs, $\ddot{\text{o}}_{\delta}o\ddot{\text{o}}_{\delta}o\ddot{\text{o}}_{\delta}$, comparable to $YBa_2Cu_3O_{6+y}$ near $y = 0.9$.

Beyond enrichment $\delta = 0.085$, where $q_c = 0.26$, no further stripes are observed in $HgBa_2CuO_{4+\delta}$. An extrapolation in Ref. 35 of X-ray data to $T_c = 95$ K, as well as Eq. (13) for $\delta = 0.10$, gives a *commensurable* value, $q_c = 0.25$ (Bragg peak). The value $q_c = 0.23$ near optimal doping ($T_c = 95$ K) from another X-ray investigation³⁶ may originate with a spurious secondary phase.³⁵ Streaks connecting the Bragg peaks for higher oxygen enrichment have been attributed to interstitial O_{δ} stripes in the $Hg-O(2)$ layers.^{36,37} However, axial stripe formation of ozone molecule ions, consisting of interstitial O_{δ} atoms between lattice-site $O(2)$ ions, is also conceivable.

XI. STRIPES IN BISMUTH-BASED CUPRATES

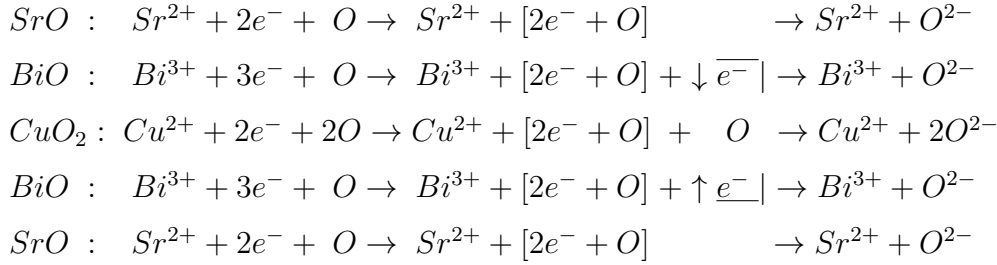
Charge-order stripes have been observed in oxygen-enriched, bismuth-based cuprates with single or double CuO_2 plane per unit cell.^{38–40} Their incommensurability, $q_c \approx 0.3$, in the bulk of CuO_2 double-plane $Bi_2Sr_2CaCu_2O_{8+\delta}$ —decreasing with more oxygen enrichment (see Table III)—is comparable to q_c of double-plane $YBa_2Cu_3O_{6+y}$. In $Bi_2Sr_{1-x}La_xCuO_{6+\delta}$, of single CuO_2 plane per unit cell, the incommensurability, $q_c \approx 0.25$, is also decreasing with super-oxygenation, and is somewhat less (by ~ 0.02) than q_c of single-plane $HgBa_2CuO_{4+\delta}$. From the absence of a square-root dependence of $q_c(\delta)$ on oxygen enrichment and from the absence of magnetization stripes, we can again infer that the stripes are formed by tilted

Compound	T_c (K)	p	q_c (r.l.u)	ξ (Å)	Ref.
$Bi_2Sr_{1-x}La_xCuO_{6+\delta}$	15	0.115	0.265	26	38
$Bi_2Sr_{1-x}La_xCuO_{6+\delta}$	22	0.130	0.257	23	38
$Bi_2Sr_{1-x}La_xCuO_{6+\delta}$	30	0.145	0.243	21	38
$Bi_2Sr_2CaCu_2O_{8+\delta}$	45	0.09	0.30	24	39
$Bi_{1.5}Pb_{0.6}Sr_{1.54}CaCu_2O_{8+\delta}$	98	0.16	0.28	< 24	40

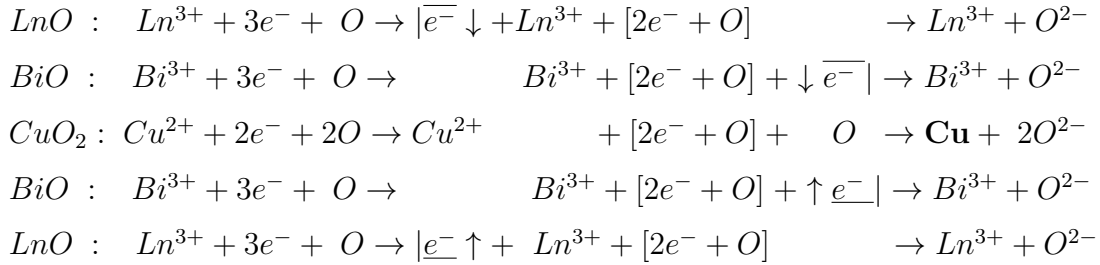
TABLE III: Incommensurability q_c of charge-order stripes in O -enriched, Bi -based cuprates with single or double CuO_2 plane. The hole density p is obtained from the transition temperature T_c with the universal-dome method (Sect. XIII). The stripes' correlation length is denoted as ξ .

ozone ions. The correlation lengths ξ from Table III indicate trains of about two tilted $\ddot{O}\ddot{O}\ddot{O}$ motifs, *viz.*, $\ddot{o}_{\ddot{o}}o\ddot{O}\ddot{o}_{\ddot{o}}o\ddot{O}\ddot{o}$.

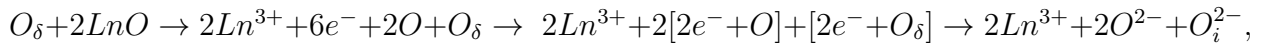
Bi-based cuprates with *double* CuO_2 plane per unit cell show typical features resulting from oxygen enrichment—as encountered in $YBa_2Cu_3O_{6+y}$ and $HgBa_2CuO_{4+\delta}$ —such as the $q_c(\delta)$ relation of Eq. (11) and the validity of the “universal-dome” method to determine the hole density $p = p(T_c)$, Sect. XIII. In contrast, superconducting *Bi*-based cuprates with *single* CuO_2 plane are more complicated, as they are not only oxygen enriched, but also *electron doped*. This can be seen in the following diagrams of stepwise ionization of $Bi_2Sr_{2-x}Ln_xCuO_{6+\delta}$ ($Ln = La, Bi$). In the *parent* crystal we have:



In the simplest case of *doping*, Ln substitutes, in some cells, Sr in both sandwiching layers:



The doped electrons reside pairwise in lattice-site Cu atoms (marked bold). At doping $x = 0.5$, an average of half an electron—or a quarter of an electron pair—reaches each unit square of the CuO_2 plane. This causes the formation of a 2×2 Cu superlattice with afm ordering of magnetic moments, $\mathbf{m}(Cu)$. Because of comparable magnitudes,¹ $|\mathbf{m}(Cu)| \approx |\mathbf{m}(Cu^{2+})|$, they perpetuate the AFM of the host crystal. There are indications^{41,42} that at less doping, $x < 0.5$, some of the excess oxygen enters the Sr/LnO layers,



where each O_{δ} atom absorbs two electrons from the $Ln \rightarrow Sr$ substitution and resides as an interstitial O_i^{2-} ion. Accordingly, only a part $\eta = \varphi x$ of the electrons, generated by

the $Ln \rightarrow Sr$ substitution, reaches the CuO_2 plane to reduce Cu^{2+} to Cu . For $Ln = Bi$, the fraction is $\varphi \simeq 0.5$. It seems energetically favorable that the 2×2 Cu superlattice still persists at doping $x < 0.5$. The lack of doped electrons from the Sr/LnO layer, necessary to reduce every fourth Cu^{2+} ion to Cu , is then made up by taking that amount from lattice-site oxygen ions, $O^{2-} - 2e^- \rightarrow O$. This amounts to *hole* doping of the CuO_2 plane with density $p = 1/4 - \varphi x$. The O lattice defects form a superlattice of their own. Their magnetic moments, $\mathbf{m}(O)$, give rise to magnetization stripes of incommensurability $q_m(p) \approx p$ —an approximation of the derived¹ square-root dependence, Eqs. (3,1), familiar from $La_{2-x}Ae_xCuO_4$. As in the latter compounds, the stripes change orientation from diagonal to axes-parallel near $p = 0.056$. Table IV shows for $Bi_2Sr_{2-x}Bi_xCuO_{6+\delta}$ the independently determined quantities $(\frac{1}{4} - \frac{x}{2}) \approx p$.

x	$\frac{1}{4} - \frac{x}{2}$	p	q_m
0.50	0.00	0.01	0.024
0.40	0.05	0.06	0.055
0.30	0.10	0.09	0.093
0.20	0.15	0.12	0.113

TABLE IV: Doping level x of $Bi_2Sr_{2-x}Bi_xCuO_{6+\delta}$, measured with inductively-coupled plasma atomic emission spectroscopy,⁴¹ hole density p , measured by Hall effect,⁴¹ and incommensurability of magnetization stripes, q_m , measured with neutron scattering.⁴¹

XII. STRIPES IN OXYGENATED $La_2CuO_{4+\delta}$ REVISITED

As reported in Sect. III, magnetization stripes with $q_m \simeq 0.115$ parallel to the $Cu-O$ bonds are observed^{22,27} in oxygen-enriched $La_2CuO_{4+\delta}$, but no accompanying charge-order stripes with $q_c = 2q_m$, as familiar from $La_{2-x}Ae_xCuO_4$. Instead, charge-order stripes are observed with $q_c = 0.15$ (in quasi-tetragonal r.l.u.) *diagonal* to the $Cu-O$ bonds.^{21,24,26} By Eqs. (3, 1), the magnetization stripes with $q_m = 0.115$ are caused by a hole density of $p = 0.12$ in the CuO_2 planes. If all of the observed excess oxygen, $y = 0.12$, were to reside ionized at $O(4)$ positions, this would result in a hole density of $p = 2\delta = 0.24$ in the CuO_2

planes. The default raises the possibility that half of the excess oxygen is embedded by a different mechanism—without magnetism but contributing to the observed charge order.

From the $La_{2-x}Ae_xCuO_4$ compounds it is known that hole doping of the CuO_2 planes saturates at a watershed value, $\hat{x} \approx 0.13$, resulting in constant $q_{c,m}(x)$ at higher Ae -doping, $x > \hat{x}$ (see Fig. 1).¹ The doped holes then start populating the LaO planes, harbored again pairwise in (lattice-site) O atoms. A similar saturation of doped holes in the CuO_2 planes may be at hand in $La_2CuO_{4+\delta}$, starting at $p \simeq 0.12 = \delta/2$ —except that the LaO planes have already excess oxygen ions, located at $O(4)$ positions. Thus, a different embedding mechanism may commence. From the experience of stripes in oxygen-enriched (Y -, Hg - or Bi -based) cuprates, embedding excess oxygen atoms at “pore” sites, $\overset{\circ}{O}$, comes to mind.

Figure 8 shows the CuO_2 plane of a model case for $La_2CuO_{4+\delta}$ with both lattice-site O atoms (dark blue) and ozone molecule ions, $\overset{\circ}{O}\overset{\circ}{O}\overset{\circ}{O}$ (turquoise). Each O atom harbors two doped holes that result from excess O_δ^{2-} at $O(4)$ positions. Coulomb repulsion spreads the lattice-defect O atoms (with their double holes) to a 4×4 superlattice. (If no $\overset{\circ}{O}\overset{\circ}{O}\overset{\circ}{O}$ ions were present, then the O superlattice would give rise to accompanying charge-order stripes parallel to the $Cu-O$ bonds with $q_c = 1/4 = 0.25$.) The $\overset{\circ}{O}\overset{\circ}{O}\overset{\circ}{O}$ ions, formed from interstitial oxygen at pore sites with oxygen neighbors, reside farthest away from the O -superlattice sites, that is, at $(a, b) = (2, 2 \pm 0.5)$ or $(2 \pm 0.5, 2)$ positions near the center of the superlattice cells—exemplified by $(2, 1.5)$ in Fig. 8. Magnetization stripes of $q_m = 1/8$ arise from the

Quantity of $La_2CuO_{4+\delta}$	Parameters observed in experiment	Ref.	Model parameters in Fig. 8
δ	0.12	22	0.1325
2δ	0.24		0.265
$q_m(\delta)$ parallel	0.115	22,27	0.125
p	0.12	Eq. (3)	0.14
$2\delta - p$	0.12		0.125
$\Omega = (2\delta - p)/2$	0.06		0.0625
$q_c(\delta)$ diagonal	0.15	21,24,26	0.177

TABLE V: Observed parameters of $La_2CuO_{4+\delta}$ (bold) and model parameters of Fig. 8. The hole density p in the CuO_2 planes is calculated from $q_m(\delta)$ with Eqs. (3, 1). Ω denotes the density of interstitial oxygen at pore sites, $\overset{\circ}{O}$.

antiferromagnetic ordering of $\mathbf{m}(O) \neq 0$ moments (red arrows in Fig. 8), whereas the ozone molecule ions have no magnetic contribution, $\mathbf{m}(\ddot{O}\ddot{O}\ddot{O}) = 0$. Approximating the ozone $(2, 2 \pm 0.5)$ and $(2 \pm 0.5, 2)$ positions by their average, $(2, 2)$, yields diagonal charge-order stripes of $q_c = 0.25/\sqrt{2} = 0.177$.

The model parameters for Fig. 8, chosen for ease of display and listed in Table V, are close to the parameters δ , q_m and q_c as experimentally observed in $La_2CuO_{4+\delta}$, although systematically larger. Accordingly, Fig. 8 gives an approximate rendition of the actual CuO_2 planes in $La_2CuO_{4+\delta}$. The density of interstitial oxygen at pore sites, \dot{O} , in $La_2CuO_{4.12}$,

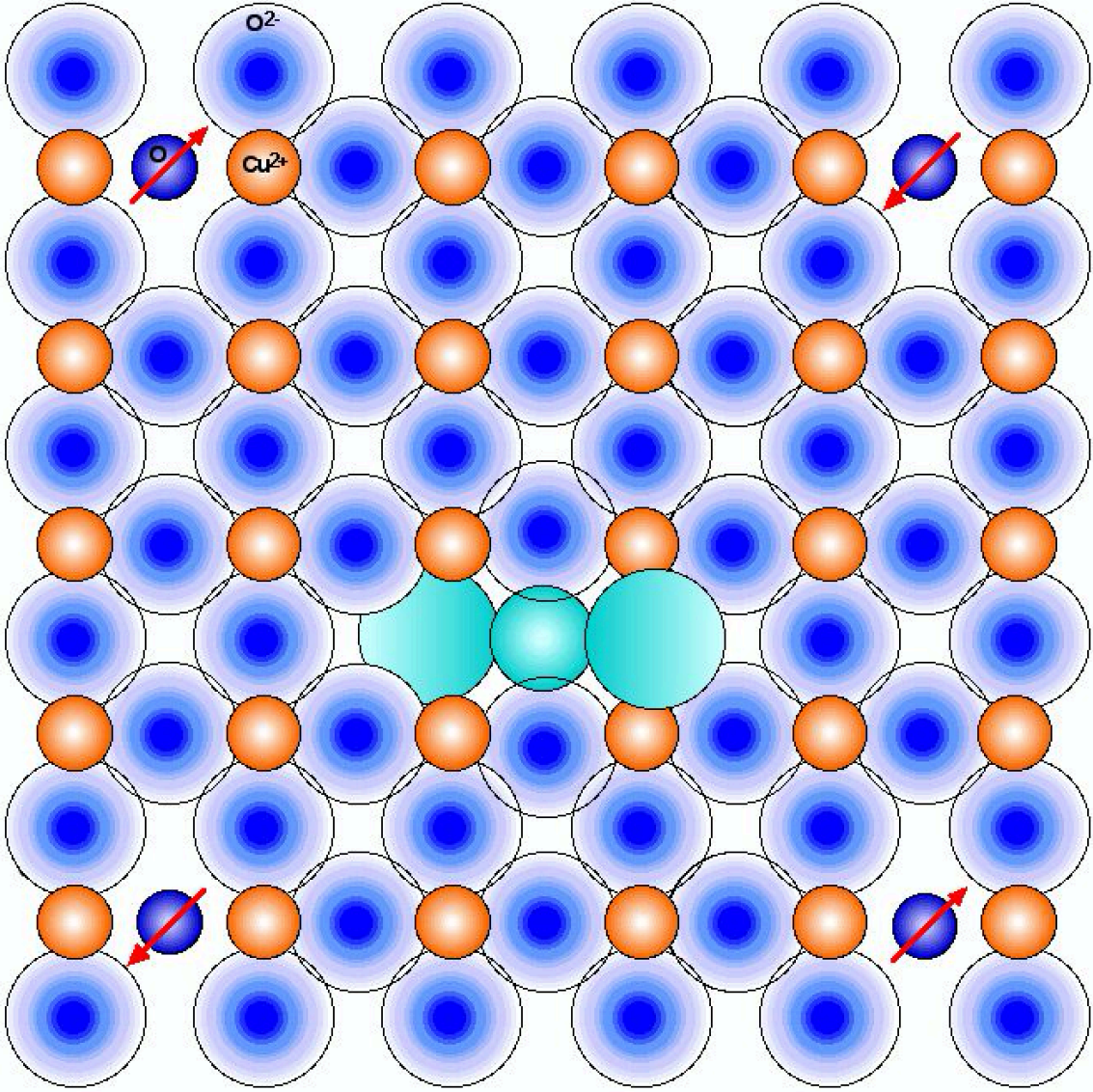


FIG. 8. CuO_2 plane of $La_2CuO_{4+\delta}$ with a 4×4 superlattice of O atoms (dark blue) and a staggered 4×4 superlattice of ozone molecule ions $\ddot{O}\ddot{O}\ddot{O}$ (turquoise). Model parameters are listed in Table V. Red arrows show the antiferromagnetic ordering of $\mathbf{m}(O)$ moments.

$\Omega = 0.06$ (Table V) is comparable with that of $YBa_2Cu_3O_{6.67}$ ($\delta = 0.06$, Table II) and $HgBa_2CuO_{4.12}$ ($\delta = 0.06$, Ref. 33). Their transition temperatures are $T_c = 42$ K, 65.5 K, and 55 K, respectively.^{28,33,43}

The finding that oxygen enrichment of $La_2CuO_{4+\delta}$ yields, besides oxygen embedding in oxygen-quartet pores, also hole doping of the CuO_2 planes may be a consequence of its staggered LaO double planes with intermediate $O(3)$ sites for O_δ^{2-} ions from oxygen enrichment. Likewise, the hole-doping contribution from *excess* oxygen in $Nd_{2-x}Ce_xCuO_{4+\delta}$ may be a consequence of their staggered NdO double planes. If this argument is valid, the *absence* of $Ln^{3+}O^{2-}$ double planes in the Y -, Hg - and Bi -based cuprates would explain their lack of lattice-site O atoms in the CuO_2 planes—and accordingly, their lack of square-root dependent stripe incommensurability $q_{c,m}(\delta)$.

XIII. HOLE DENSITY IN THE CuO_2 PLANES

Shortly after the discovery⁴⁴ of high- T_c superconductivity in $La_{2-x}Ba_xCuO_4$, various theories were proposed (reviewed in Ref. 45). They all share the view that high- T_c superconductivity arises when the CuO_2 planes are doped with holes. Some of the initial theories were discarded quickly because crucial predictions were falsified by experiment. Interest in other initial theories has waned over the decades. Nevertheless, the notion of “doped holes in the CuO_2 planes” is commonly held. Backed by stoichiometry and charge balance, the notion clearly holds for $La_{2-x}Ae_xCuO_4$, with hole density $p = x$. But what is p in $YBa_2Cu_3O_{6+y}$, with its CuO chains, and in the non-stoichiometric, oxygen-enriched cuprates, generated by diffusion and thermal procedures? Here, a claim of universal $T_c(p)$ dependence has been resorted to.⁴⁶ Neglecting the deep chasm in the $T_c(p)$ profile of $La_{2-x}Ba_xCuO_4$ at $x = 1/8$, and the dent in $T_c(p)$ of $La_{2-x}Sr_xCuO_4$ near $x = 1/8$, the profile, also called the “superconducting dome,” has been modelled as

$$\frac{T_c(p)}{T_{c,max}} = 1 - \frac{(p - p_{opt}^{SC})^2}{(p_{ons}^{SC} - p_{opt}^{SC})^2} = 1 - 82.6(p - 0.16)^2, \quad (14)$$

with maximal transition temperature at optimal doping, $T_c(p_{opt}^{SC}) = T_{c,max}$, and onset of superconductivity, $T_c(p_{ons}^{SC}) = 0$ (see Fig. 9). The onset and optimal doping, $p_{ons}^{SC} \simeq 0.05$ and $p_{opt}^{SC} \simeq 0.16$, were obtained from $La_{2-x}Sr_xCuO_4$. This gives the formula on the right of Eq. (14). Inverting the formula furnishes the underdoped (*ud*) and overdoped (*od*) hole density

in the CuO_2 plane as

$$p_{ud}^{od}(T_c) = 0.16 \pm \sqrt{\frac{T_{c,max} - T_c}{82.6 T_{c,max}}}, \quad (15)$$

in terms of the observed T_c and $T_{c,max}$. Such p values have been widely used to characterize the doping dependence of stripe incommensurability $q_c(p)$ and of other properties in the pseudogap phase of oxygen-enriched cuprates [later with a more accurate value $p_{ons}^{SC} \simeq 0.056$, which changes the coefficient 82.6 in Eqs.(14, 15) to 91.67].

The universal-dome method—proposed half a decade before charge-order stripes were discovered⁴⁷ in $La_{1.6-x}Nd_{0.4}Sr_xCuO_4$ and (another decade and a half later)^{7,8} in $YBa_2Cu_3O_{6+y}$ —assumes that the *same* mechanism of high- T_c superconduction holds both in heterovalent metal-doped, and in oxygen-doped/enriched cuprates. There is no *a priori* reason why this should be the case.

What both compound families have in common are CuO_2 planes with lattice-defect *oxygen atoms*. Where the two groups differ is the *location* of those atoms—either at anion lattice sites, O (besides skirmishing oxygen atoms, \tilde{O}), or at interstitial sites, \dot{O} , with respective defect-charges $Q(O) = +2|e|$ but $Q(\dot{O}) = 0$ (relative to the host crystal, see Appendix A) and magnetic moments $|\mathbf{m}(O)| \neq 0$ but $|\mathbf{m}(\ddot{O}\ddot{O})| = 0$. The lack of electron transfer from LaO to CuO_2 planes in the crystal formation of $La_{2-x}Ae_xCuO_4$ (illustrated in Sect. II) can

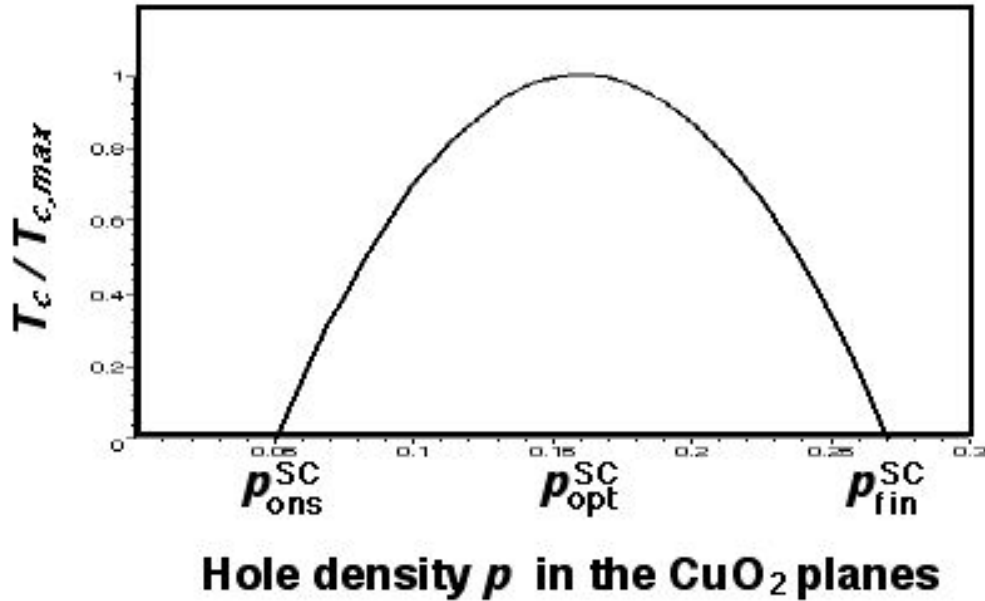


FIG. 9. Universal dome, $T_c(p)$, of superconducting cuprates, Eq. (14).

be regarded as “hole doping.” Since the holes reside pairwise in oxygen atoms, we may extend the notion to “oxygen-atom doping” of the CuO_2 planes, with densities

$$p(y) = 2\delta(y), \quad (16)$$

respectively. Values of $\delta(y)$ and $p(y)$ for $YBa_2Cu_3O_{6+y}$ are listed in Table II. The oxygen-atom density $\delta(y)$ is obtained with Eq. (11) from stripe data, together with two family-specific parameters [$\delta(y_c^{ons})$ and $\gamma = dq_c/d\delta$]. Conversely, the hole density p is obtained from superconducting transition temperatures with the universal-dome method, Eq. (15). Derived independently, the $\delta(y)$ and $p(y)$ values from Table II satisfy Eq. (16). The agreement has an important implication for the mechanism of high- T_c superconductivity in cuprates, discussed in Sect. XIV.

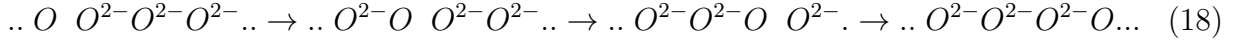
Not quite as sure-footed is the universal-dome method for $HgBa_2CuO_{4+\delta}$. Although the onset of superconductivity³³ is also at $2\delta_{ons}^{SC} = p = 0.05$, the optimal doping is somewhat uncertain, with $\delta_{opt}^{SC} = 0.13 \pm 0.01$ from neutron-scattering experiments but $\delta_{opt}^{SC} = 0.16$ from thermoelectric-power investigations.^{33,48} For *Bi*-based cuprates with two CuO_2 planes per unit cell, such as $Bi_2Sr_2CaCu_2O_{8+\delta}$, the universal-dome method seems quite reliable and is widely used.^{49–51} Conversely, the universal-dome method is not applicable to single-plane $Bi_2Sr_{2-x}Ln_xCuO_{6+\delta}$ ($Ln = La, Bi$), because of both oxygen enrichment and electron doping by $Ln \rightarrow Sr$ substitution. Instead, the carrier density is obtained from the size of the Fermi surface (Luttinger theorem).^{42,52,53}

XIV. IMPLICATIONS FOR SUPERCONDUCTIVITY

Although details are not clear, it seems a fairly safe assumption that neutral oxygen atoms in the CuO_2 planes affect superconductivity. Just as they give rise to different types of stripes, depending on their position—and position-related properties (lattice-defect charge, magnetic moment)—they may likewise give rise to different types of superconductivity. A possibility that comes to mind is that in *oxygen-doped/enriched* cuprates, superconducting (Cooper) *pairs* of holes, $2e_{\uparrow\downarrow}^+$, progress by successively moving from interstitial $\overset{\circ}{O}$ atoms to neighboring O^{2-} ions, turning them to $\overset{\circ}{O}$ atoms, *etc.*,

$$.. \overset{\circ}{O} O^{2-} O^{2-} O^{2-} .. \rightarrow .. O^{2-} \overset{\circ}{O} O^{2-} O^{2-} .. \rightarrow .. O^{2-} O^{2-} \overset{\circ}{O} O^{2-} .. \rightarrow .. O^{2-} O^{2-} O^{2-} \overset{\circ}{O} .. \quad (17)$$

The spin-singlet configuration ($S = 0$) of the hole pair, indicated by the subscript-arrows, and in agreement with the $\overset{\circ}{O}$ atom (more accurately, of the $\overset{\circ}{O}\overset{\circ}{O}\overset{\circ}{O}$ ion), gives it a spin-magnetic moment $\mathbf{m}_s(2e_{\uparrow\downarrow}^+) = \mathbf{m}_s(\overset{\circ}{O}\overset{\circ}{O}\overset{\circ}{O}) = 0$. On the other hand, in Ae -doped lanthanum cuprates, superconducting pairs of doped holes, $2e_{\uparrow\uparrow}^+$, progress by successively moving from anion-site O atoms to neighboring O^{2-} ions,



Here each hole pair, $2e_{\uparrow\uparrow}^+$, has a spin-magnetic moment $\mathbf{m}_s = 2\mu_B$ (spin-triplet configuration, $S = 1$).

It turns out that some properties of superconductivity are the same for both processes, (17, 18), but others are different. The universal-dome method obtains the doping of superconductivity onset, $p_{ons}^{SC} = 0.05$, and the optimal doping, $p_{opt}^{SC} = 0.16$ of oxygen-doped/enriched cuprates by adopting those of $La_{2-x}Sr_xCuO_4$. It is found that the resulting p values agree, for $YBa_2Cu_3O_{6+y}$, with (twice) the $\delta(y)$ values obtained independently from $YBa_2Cu_3O_{6+y}$ stripe data (Table II). This confirms that the oxygen-atom doping for onset and maximal superconductivity is the *same* for both compound families, $x_{ons}^{SC} = p_{ons}^{SC} = 2\delta_{ons}^{SC} = 0.05$ and $x_{opt}^{SC} = p_{opt}^{SC} = 2\delta_{opt}^{SC} = 0.16$. As far as the onset and maximum of superconductivity are concerned, the exact location of the oxygen atoms in the CuO_2 planes does not matter: A threshold density of oxygen atoms is necessary to get superconductivity going, regardless of their exact position. Likewise, maximal *relative* transition temperature $T_c/T_{c,max}$ is achieved at optimal density.

A quantity that is *different* for the processes (17, 18) is the *absolute* transition temperature, T_c . Because of their magnetic moment $\mathbf{m}_s = 2\mu_B$, the $2e_{\uparrow\uparrow}^+$ hole pairs in process (18) are susceptible to disturbance from magnetic deviations in the crystal, such as magnetization

Compound	S	$T_{c,max}$	Ref.	Comment
$HgBa_2CuO_{4+\delta}$	0	95 K	35	no magnetization stripes
$La_{2-x}Sr_xCuO_4$	1	36 K	43	magnetization stripes
$La_{1.6-x}Nd_{0.4}Sr_xCuO_4$	1	15 K	54	magn. stripes + $\mathbf{m}(Nd^{3+})$ moments

TABLE VI: Maximal transition temperature, $T_{c,max}$, of compounds with a single CuO_2 plane per unit cell. S is the spin quantum number of the superconducting hole pair.

stripes and magnetic impurities. This would lower the transition temperature of compounds with spin-triplet pairs (18), compared to those with spin-singlet pairs (17). The maximal transition temperatures of comparable compounds with a single CuO_2 plane per unit cell, listed in Table VI, show clear differences. The temperature $T_{c,max}$ is highest for the oxygen-enriched compound ($S = 0$) where magnetization stripes are absent. It is much lower for magnetic hole pairs ($S = 1$) when subject to magnetization stripes, and still lower when irregularly positioned magnetic moments (from Nd^{3+} with $4f^3$ subshell) are present.

Another superconducting property that is *different* in the two compound families concerns the cooling-curve of X-ray intensity diffracted by charge-order stripes at temperatures *below* T_c . The superconducting hole pairs that don't participate in a supercurrent, *fluctuate* about average positions. In $La_{2-x}Ae_xCuO_4$, Coulomb repulsion keeps $2e_{\uparrow\downarrow}^+$ pairs fluctuating about the O superlattice sites, as can be concluded from the same value of incommensurability, $q_{c,m}(x)$, above and below T_c . In contrast, superconducting fluctuations of $2e_{\uparrow\downarrow}^+$ pairs in oxygen-doped/enriched cuprates loosen the axial cohesion between $\ddot{O}\ddot{O}\ddot{O}\ddot{O}$ motifs. The latter then disperse, causing weaker charge-order stripe-intensity, in thermodynamic proportion of the superconducting/normal states (Gorter-Casimir two-fluid model of superconductivity). This can be inferred from cooling-curves, shown schematically in Fig. 10.

Such cooling-curves are distinctly different for $La_{2-x}Ae_xCuO_4$ and $YBa_2Cu_3O_{6+y}$. The signal from $La_{2-x}Ae_xCuO_4$ samples rises continuously with cooling through, and below T_c , for Ae -doping below the watershed value, $x < \hat{x}$. The reason is decreasing thermal agitation, causing increasing coherence length.¹ For $x > \hat{x}$, superconducting fluctuations of O atoms

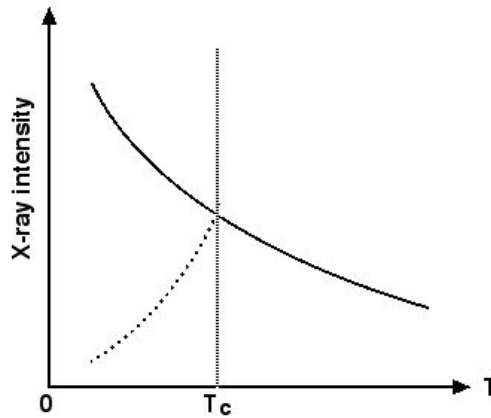


FIG. 10. Cooling-curves (schematic) of X-ray intensity diffracted by charge-order stripes in the CuO_2 planes: Below T_c , they are *falling* for $YBa_2Cu_3O_{6+y}$, $Bi_2Sr_2CaCu_2O_{8+\delta}$ and $La_{2-x}Ae_xCuO_4$ ($Ae = Sr, Ba$) if $x > \hat{x}$; but they are *rising* for $La_{2-x}Ae_xCuO_4$ when doped below a watershed value, $x < \hat{x} \approx 0.13$.

to the LaO planes reduces their (average) presence in the CuO_2 planes. This reduces the X-ray signal and causes a falling cooling curve below T_c .¹ Mixed results of cooling-curves in *early* experiments on $La_{2-x}Ae_xCuO_4$ have recently been clarified, as discussed in Ref. 1.

In $YBa_2Cu_3O_{6+y}$ above T_c , the cooling-curve also keeps rising upon cooling, due to lesser thermal agitation. However, the curve culminates in a *cusp* at T_c . Further cooling leads to a *falling* cooling-curve due to gradual dissolution of the stripe-forming $\ddot{O}\ddot{O}\ddot{O}$ trains to isolated $\ddot{O}\ddot{O}$ molecule ions. From a formal perspective, a falling cooling-curve is conventionally regarded as a competition of (stripe- *vs.* superconducting) order parameters. In the present microscopic view, the falling cooling-curve of $YBa_2Cu_3O_{6+y}$ and $Bi_2Sr_2CaCu_2O_{8+\delta}$ (charge-order “melting”)^{7,8,55} is interpreted as a consequence of quantum fluctuations of $2e_{\uparrow\downarrow}^+$ pairs that loosen the axial cohesion between $\ddot{O}\ddot{O}\ddot{O}$ motifs. The same quantum fluctuations also “soften” bond-stretching phonons by decreasing, in Fano-like interference, their frequency at the reciprocal-lattice value of charge-order incommensurability, $\omega(q_c)$.^{55,56}

XV. CONCLUSION

Charge-order stripes of different types occur when copper oxides are doped either with heterovalent metal, like $La_{2-x}Sr_xCuO_4$, or oxygen doped, like $YBa_2Cu_3O_{6+y}$. The difference shows up in the doping dependence of their incommensurability: $q_c(x) \propto \sqrt{x - \bar{p}}$ but $q_c(y) \approx 0.3$. The square-root dependence in the former compound family results from Coulomb repulsion between doped holes, residing pairwise in lattice-site O atoms in the CuO_2 planes (or between doped electrons, residing pairwise in lattice-site Cu atoms, as in $Nd_{2-x}Ce_xCuO_4$). The almost constant $q_c(y)$ value in the second family—decreasing slightly with more oxygen doping—results from the aggregation of ozone-like molecules, $\ddot{O}\ddot{O}$, formed from O^{2-} ions of the host with embedded oxygen atoms, \ddot{O} , at interstitial sites in the CuO_2 planes. The magnetic moments, $\mathbf{m}(O)$, of the lattice-defect O atoms in the first family arrange antiferromagnetically, which gives rise to accompanying magnetization stripes of incommensurability $q_m(x) = \frac{1}{2}q_c(x)$. The ozone complexes have a vanishing magnetic moment, $\mathbf{m}(\ddot{O}\ddot{O}) = 0$, which explains the absence of accompanying magnetization stripes in the second family. Embedding of excess oxygen atoms in “pores” of CuO_2 planes is likewise assumed for $HgBa_2CuO_{4+\delta}$ and oxygen-enriched bismuth cuprates. A combination of characteristics from both families is present in oxygen-enriched La_2CuO_{4+y} , with both

hole doping and ozone complexes, possibly as a consequence of the LaO double layers. The validity of the universal-dome method to determine the hole density, p , of oxygen-enriched cuprates (not co-doped with electrons) is independently confirmed. Besides causing different types of stripes, the two types of lattice-defect oxygen, O or $\overset{\circ}{O}$, may also cause different types of superconductivity. This could explain the much higher transition temperature $T_{c,max}$ in oxygen-enriched than Ae -doped cuprates, as well as the cusped cooling-curves of X-ray intensity diffracted by stripes in the former family.

Appendix A: LATTICE-DEFECT CHARGE

Besides short-range repulsion (due to Pauli's exclusion principle) and van der Waals attraction (from fluctuating dipoles), long-range *Coulomb* interaction contributes to the lattice energy by the Madelung term,

$$U^{Mad} = \sum_j^{cell} Q(j) V(\overset{j}{site}), \quad (A1)$$

summed over the atoms of a unit cell. Here $Q(j)$ is the electric charge of atom j and $V(\overset{j}{site})$ is the Madelung potential at the position of j . We denote a lattice-defect oxygen atom at an anion lattice site in the CuO_2 plane of $La_{2-x}Ae_xCuO_4$ by underline, \underline{O} . Its contribution to the Madelung energy is

$$\Delta U_{an-sit}^{Mad}(\underline{O}) = Q(\underline{O}) V(\overset{anion}{site}) = 0 \times V(\overset{anion}{site}) = 0. \quad (A2)$$

Compared to the corresponding contribution of an \underline{O}^{2-} ion in the La_2CuO_4 host crystal,

$$\Delta U_{an-sit}^{Mad}(\underline{O}^{2-}) = Q(\underline{O}^{2-}) V(\overset{anion}{site}) = -2|e| \times V(\overset{anion}{site}), \quad (A3)$$

the contribution of the lattice-defect \underline{O} atom, Eq. (A2), is

$$\Delta U_{an-sit}^{Mad}(\underline{O}) = \Delta U_{an-sit}^{Mad}(\underline{O}^{2-}) + 2|e| \times V(\overset{anion}{site}). \quad (A4)$$

Thus, *relative* to the La_2CuO_4 host, a neutral oxygen atom at an anion site appears as if it has a *positive* lattice-defect charge $Q(\underline{O}) = +2|e|$.

Applying the same rationale to an oxygen atom at an interstitial ‘‘pore’’ site, $\overset{\circ}{O}$, we have

$$\Delta U_{po-sit}^{Mad}(\overset{\circ}{O}) = Q(\overset{\circ}{O}) V(\overset{pore}{site}) = 0 \times V(\overset{pore}{site}) = 0. \quad (A5)$$

Since interstitial sites are not occupied in pristine La_2CuO_4 , there is no such contribution in the host crystal,

$$\Delta U_{po-sit}^{Mad}(\) = 0. \quad (\text{A6})$$

Thus, the *interstitial* atom at the ‘‘pore’’ site, \mathring{O} , has the same lattice-defect charge, relative to the host crystal, as its real charge, $Q(\mathring{O}) = Q(O) = 0$.

Appendix B: PARAMETERS OF $YBa_2Cu_3O_{6+y}$ MAGNETIZATION STRIPES

Squaring Eq. (7) gives, after rearrangement,

$$\frac{16}{g}q_m^2(y) = y - \check{y}. \quad (\text{B1})$$

Omitting the magnetization suffix m , we label the three oxygen doping levels as y_i , y_j and y_k and the corresponding incommensurabilities as q_i , q_j and q_k . Insertion into Eq. (B1), yields

$$\frac{16}{g}q_i^2 = y_i - \check{y}, \quad (\text{B2})$$

$$\frac{16}{g}q_j^2 = y_j - \check{y}, \quad (\text{B3})$$

$$\frac{16}{g}q_k^2 = y_k - \check{y}. \quad (\text{B4})$$

We add Eqs. (B2) and (B3) to obtain, after rearrangement,

$$2\check{y} = y_i + y_j - \frac{16}{g}(q_i^2 + q_j^2). \quad (\text{B5})$$

Substituting g from Eq. (B4) and rearranging yields

$$\check{y}\left(2 - \frac{q_i^2 + q_j^2}{q_k^2}\right) = y_i + y_j - y_k \frac{q_i^2 + q_j^2}{q_k^2}. \quad (\text{B6})$$

Using the experimental data,⁴ $q_i(0.30) = 0.02$, $q_j(0.35) = 0.028$ and $q_k(0.45) = 0.045$, we calculate $\check{y} = 0.27$. Insertion of \check{y} into Eq. (B4) gives

$$g = 16 \frac{q_k^2}{y_k - \check{y}} \quad (\text{B7})$$

with a numerical value $g = 0.18$.

ACKNOWLEDGMENTS

I thank Wojciech Tabis and Neven Barišić for information and literature references related to $HgBa_2CuO_{4+\delta}$. Thanks also to Antonio Bianconi for information and literature references on $La_2CuO_{4+\delta}$.

-
- ¹ M. Bucher, “Stripes in heterovalent-metal doped cuprates,” arXiv:2002.12116v6
- ² V. Hinkov, D. Haug, B. Fauqué, P. Bourges, Y. Sidis, A. Ivanov, C. Bernhard, C. T. Lin, and B. Keimer, *Science* **319**, 597 (2008).
- ³ D. Haug, V. Hinkov, A. Suchaneck, D. S. Inosov, N. B. Christensen, Ch. Niedermayer, P. Bourges, Y. Sidis, J. T. Park, A. Ivanov, C. T. Lin, J. Mesot, and B. Keimer, *Phys. Rev. Lett.* **103**, 017001 (2009).
- ⁴ D. Haug, V. Hinkov, Y. Sidis, P. Bourges, N. B. Christensen, A. Ivanov, T. Keller, C. T. Lin, and B. Keimer, *New J. Phys.* **12**, 105006 (2010).
- ⁵ V. Hinkov, C.T. Lin, M. Raichle, B. Keimer, Y. Sidis, P. Bourges, S. Pailhès, and A. Ivanov, *Eur. Phys. J. - Special Topics* **188**, 113 (2010).
- ⁶ Z. Yamani, W. J. L. Buyers, F. Wang, Y.-J. Kim, J.-H. Chung, S. Chang, P. M. Gehring, G. Gasparovic, C. Stock, C. L. Broholm, J. C. Baglo, R. Liang, D. A. Bonn, and W. N. Hardy, *Phys. Rev. B* **91**, 134427 (2015).
- ⁷ G. Ghiringhelli, M. Le Tacon, M. Minola, S. Blanco-Canosa, C. Mazzoli, N. B. Brookes, G. M. De Luca, A. Frano, D. G. Hawthorn, F. He, T. Loew, M. Moretti Sala, D. C. Peets, M. Salluzzo, E. Schierle, R. Sutarto, G. A. Sawatzky, E. Weschke, B. Keimer, L. Braicovich, *Science*, **337**, 821 (2012).
- ⁸ J. Chang, E. Blackburn, A. T. Holmes, N. B. Christensen, J. Larsen, J. Mesot, R. Liang, D. A. Bonn, W. N. Hardy, A. Watenphul, M. v. Zimmermann, E. M. Forgan, and S. M. Hayden, *Nature Physics*, **8**, 871 (2012).
- ⁹ A. J. Achkar, R. Sutarto, X. Mao, F. He, A. Frano, S. Blanco-Canosa, M. Le Tacon, G. Ghiringhelli, L. Braicovich, M. Minola, M. Moretti Sala, C. Mazzoli, R. Liang, D. A. Bonn, W. N. Hardy, B. Keimer, G. A. Sawatzky, and D. G. Hawthorn, *Phys. Rev. Lett.* **109**, 167001 (2012).
- ¹⁰ E. Blackburn, J. Chang, M. Hücker, A. T. Holmes, N. B. Christensen, R. Liang, D. A. Bonn, W. N. Hardy, U. Rütt, O. Gutowski, M. v. Zimmermann, E. M. Forgan, and S. M. Hayden, *Phys. Rev. Lett.* **110**, 137004 (2013).
- ¹¹ S. Blanco-Canosa, A. Frano, T. Loew, Y. Lu, J. Porras, G. Ghiringhelli, M. Minola, C. Mazzoli, L. Braicovich, E. Schierle, E. Weschke, M. Le Tacon, and B. Keimer, *Phys. Rev. Lett.* **110**, 187001 (2013).

- ¹² E. Blackburn, J. Chang, A. H. Said, B. M. Leu, R. Liang, D. A. Bonn, W. N. Hardy, E. M. Forgan, and S. M. Hayden, Phys. Rev. B **88**, 054506 (2013).
- ¹³ A. J. Achkar, X. Mao, C. McMahon, R. Sutarto, F. He, R. Liang, D. A. Bonn, W. N. Hardy, and D. G. Hawthorn, Phys. Rev. Lett. **113**, 107002 (2014).
- ¹⁴ S. Blanco-Canosa, A. Frano, E. Schierle, J. Porras, T. Loew, M. Minola, M. Bluschke, E. Weschke, B. Keimer, and M. Le Tacon, Phys. Rev. B **90**, 054513 (2014).
- ¹⁵ M. Hücker, N. B. Christensen, A. T. Holmes, E. Blackburn, E. M. Forgan, R. Liang, D. A. Bonn, W. N. Hardy, O. Gutowski, M. v. Zimmermann, S. M. Hayden, and J. Chang, Phys. Rev. B **90**, 054514 (2014).
- ¹⁶ R. Comin, R. Sutarto, E. H. da Silva Neto, L. Chauviere, R. Liang, W. N. Hardy, D. A. Bonn, F. He, G. A. Sawatzky, and A. Damascelli, Science **347**, 1335 (2015).
- ¹⁷ E. M. Forgan, E. Blackburn, A. T. Holmes, A. K. R. Briffa, J. Chang, L. Bouchenoire, S. D. Brown, R. Liang, D. Bonn, W. N. Hardy, N. B. Christensen, M. v. Zimmermann, M. Hücker, and S. M. Hayden, Nature Commun. **6**, 10064 (2015).
- ¹⁸ N. P. Armitage, P. Fournier, and R. L. Greene, Rev. Mod. Phys. **82**, 2421 (2010).
- ¹⁹ K. Ishii, S. Asano, M. Ashida, M. Fujita, B. Yu, M. Greven, J. Okamoto, D.-J. Huang, and J. Mizuki, “Post-growth annealing effects on charge and spin excitations in $Nd_{2-x}Ce_xCuO_4$,” arXiv:2008.03420
- ²⁰ C. Chailout, J. Chenavas, S. W. Cheong, Z. Fisk, M. Marezio, B. Morosin, and J. E. Schirber, Physica C **170**, 87 (1990).
- ²¹ A. Lanzara, N. L. Saini, A. Bianconi, J. L. Hazemann, Y. Soldo, F. C. Chou, and D. C. Johnston, Phys. Rev. **55**, 9120 (1997).
- ²² Y. S. Lee, R. J. Birgeneau, M. A. Kastner, Y. Endoh, S. Wakimoto, K. Yamada, R. W. Erwin and S.-H. Lee, and G. Shirane, Phys. Rev. B **60**, 3643 (1999).
- ²³ M. Fratini, N. Poccia, A. Ricci, G. Campi, M. Burghammer, G. Aeppli, and A. Bianconi, Nature **466**, 841 (2010).
- ²⁴ N. Poccia, A. Ricci, G. Campi, M. Fratini, A. Puri, D. Di Gioacchino, A. Marcelli, M. Reynolds, M. Burghammer, N. L. Saini, G. Aeppli, and A. Bianconi, Proc. Natl. Acad. Sci. **109**, 15685 (2012).
- ²⁵ N. Poccia, A. Ricci, G. Campi, and A. Bianconi, Supercond. Sci. Technol. **30**, 035016 (2017).
- ²⁶ N. Poccia, , M. Chorro, , A. Ricci, W. Xu, A. Marcelli, G. Campi, and A. Bianconi, Appl. Phys.

- Lett. **104**, 221903 (2014).
- ²⁷ H. Jacobsen, S. L. Holm, M.-E. Lăcătușu, A. T. Rømer, M. Bertelsen, M. Boehm, R. Toft-Petersen, J.-C. Grivel, S. B. Emery, L. Udby, B. O. Wells, and K. Lefmann, Phys. Rev. Lett. **120**, 037003 (2018).
- ²⁸ A.-E. Țuțueanu, H. Jacobsen, P. J. Ray, S. Holm-Dahlin, M.-E. Lăcătușu, T. B. Tejsner, J.-C. Grivel, W. Schmidt, R. Toft-Petersen, P. Steffens, M. Boehm, B. Wells, L. Udby, K. Lefmann, and A. T. Rømer, “Nature of the magnetic stripes in fully oxygenated La_2CuO_{4+y} ”, arXiv:2008.11527
- ²⁹ M. v. Zimmermann, J. R. Schneider, T. Frello, N. H. Andersen, J. Madsen, M. Käll, H. F. Poulsen, R. Liang, P. Dosanjh, and W. N. Hardy, Phys. Rev. B **68**, 104515 (2003).
- ³⁰ R. Liang, D. A. Bonn, and W. N. Hardy, Physica C **336**, 57 (2000).
- ³¹ H.-H. Kim, E. Lefrançois, K. Kummer, R. Fumagalli, N. B. Brookes, D. Betto, S. Nakata, M. Tortora, J. Porras, T. Loew, M. Barber, L. Braicovich, A.P. Mackenzie, C. W. Hicks, B. Keimer, M. Minola, and M. Le Tacon, “Charge density waves in $YBa_2Cu_3O_{6.67}$ probed by resonant X-ray scattering under uniaxial compression,” arXiv:2009.00928
- ³² V. L. Aksenov, A. M. Balagurov, V. V. Sikolenko, V. G. Simkin, V. A. Alyoshin, E. V. Antipov, A. A. Gippius, D. A. Mikhailova, S. N. Putilin, and F. Bouree, Phys. Rev. B **55**, 3966 (1997).
- ³³ A. M. Balagurov, D. V. Sheptyakov, V. L. Aksenov, E. V. Antipov, S. N. Putilin, P. G. Radaelli, and M. Marezio Phys. Rev. B **59**, 7209 (1999).
- ³⁴ J. P. Hodges, I. Gameson, P. P. Edwards, A. P. Kharel, and A. Porch, Phys. Rev. B **55**, 12776 (1997).
- ³⁵ W. Tabis, B. Yu, I. Bialo, M. Bluschke, T. Kolodziej, A. Kozłowski, E. Blackburn, K. Sen, E. M. Forgan, M. v. Zimmermann, Y. Tang, E. Weschke, B. Vignolle, M. Hepting, H. Gretarsson, R. Sutarto, F. He, M. Le Tacon, N. Barišić, G. Yu, and M. Greven, Phys. Rev. B **96**, 134510(2017).
- ³⁶ G. Campi, A. Bianconi, N. Poccia, G. Bianconi, L. Barba, G. Arrighetti, D. Innocenti, J. Karpinski, N. D. Zhigadlo, S. M. Kazakov, M. Burghammer, M. v. Zimmermann, M. Sprung, and A. Ricci, Nature **525**, 359 (2015).
- ³⁷ M. Izquierdo, S. Megtert, D. Colson, V. Honkimäki, A. Forget, H. Raffy, and R. Comès, J. Phys. Chem. Solids **72**, 545 (2011).
- ³⁸ R. Comin, A. Frano, M. M. Yee, Y. Yoshida, H. Eisaki, E. Schierle, E. Weschke, R. Sutarto, F. He, A. Soumyanarayanan, Y. He, M. Le Tacon, I. S. Elfimov, J. E. Hoffman, G. A. Sawatzky,

- B. Keimer, and A. Damascelli, *Science*, **343**, 390 (2014).
- ³⁹ E. H. da Silva Neto, P. Aynajian, A. Frano, R. Comin, E. Schierle, E. Weschke, A. Gyenis, J. Wen, J. Schneeloch, Z. Xu, S. Ono, G. Gu, M. Le Tacon, and A. Yazdani, *Science*, **343**, 393 (2014).
- ⁴⁰ M. Hashimoto, G. Ghiringhelli, W.-S. Lee, G. Dellea, A. Amorese, C. Mazzoli, K. Kummer, N. B. Brookes, B. Moritz, Y. Yoshida, H. Eisaki, Z. Hussain, T. P. Devereaux, Z.-X. Shen, and L. Braicovich *Phys. Rev. B* **89**, 220511(R) (2014).
- ⁴¹ M. Enoki, M. Fujita, T. Nishizaki, S. Iikubo, D. K. Singh, S. Chang, J. M. Tranquada, and K. Yamada, *Phys. Rev. Lett.* **110**, 017004 (2013).
- ⁴² Z.-H. Pan, P. Richard, Y.-M. Xu, M. Neupane, P. Bishay, A. V. Fedorov, H. Luo, L. Fang, H.-H. Wen, Z. Wang, and H. Ding, *Phys. Rev. B* **79**, 092507 (2009).
- ⁴³ H. Takagi, T. Ido, S. Ishibashi, M. Uota, S. Uchida, and Y. Tokura, *Phys. Rev. B* **40**, 2254 (1989).
- ⁴⁴ G. Bednorz and K. A. Mueller, *Z. Phys. B* **64**, 189 (1986).
- ⁴⁵ P. Lederer, “The Battle of High Temperature Superconductivity”, arXiv:1510.08808v2
- ⁴⁶ M. R. Presland, J. L. Tallon, R. G. Buckley, R. S. Liu, and N. E. Flower, *Physica C* **176**, 95 (1991).
- ⁴⁷ J. M. Tranquada, B. J. Sternlieb, J. D. Axe, Y. Nakamura, and S. Uchida, *Nature* **375**, 561 (1995).
- ⁴⁸ A. Yamamoto, W.-Z. Hu, and S. Tajima, *Phys. Rev. B* **63**, 024504 (2000).
- ⁴⁹ L. F. Lopes, J. P. Peña, M. A. Tumelero, J. Schaf, V. N. Vieira, P. Pureur, “Effects of the pseudo-gap on the field-induced kinetic energy density of $Bi_2Sr_2CaCu_2O_{8+\delta}$ single crystals,” arXiv:2008.10674
- ⁵⁰ Q. Gao, L. Zhao, C. Hu, H. Yan, H. Chen, Y. Cai, C. Li, P. Ai, J. Liu, J. Huang, H. Rong, C. Song, C. Yin, Q. Wang, Y. Huang, G. Liu, Z. Xu and X. J. Zhou, *Chinese Phys. Lett.* **37**, 087402 (2020).
- ⁵¹ Y. He, S.-D. Chen, Z.-X. Li, D. Zhao, D. Song, Y. Yoshida, H. Eisaki, T. Wu, X.-H. Chen, D.-H. Lu, C. Meingast, R. J. Birgeneau, T. P. Devereaux, M. Hashimoto, D.-H. Lee, and Z.-X. Shen, “Fluctuating superconductivity in overdoped cuprate with a flat antinodal dispersion,” arXiv:2009.10932
- ⁵² T. Kondo, T. Takeuchi, T. Yokoya, S. Tsuda, S. Shin, U. Mizutani, *J. Electron Spectroscopy*

and Related Phenomena **137–140**, 663 (2004).

- ⁵³ M. Lizaire, A. Legros, A. Gourgout, S. Benhabib, S. Badoux, F. Laliberté, M.-E. Boulanger, A. Ataei, G. Grissonnanche, D. LeBoeuf, S. Licciardello, S. Wiedmann, S. Ono, S. Kawasaki, G.-Q. Zheng, N. Doiron-Leyraud, C. Proust, and L. Taillefer, “Transport signatures of the pseudogap critical point in the cuprate superconductor $Bi_2Sr_{2-x}La_xCuO_{6+\delta}$,” arXiv:2008.13692
- ⁵⁴ M. Dragomir, Q. Ma, J. P. Clancy, A. Ataei, P. A. Dube, S. Sharma, A. Huq, H. A. Dabkowska, L. Taillefer, and B. D. Gaulin, “Materials preparation, single crystal growth, and the phase diagram of the cuprate high temperature superconductor $La_{1.6-x}Nd_{0.4}Sr_xCuO_4$,” arXiv:2008.07573
- ⁵⁵ W. S. Lee, K. J. Zhou, M. Hepting, J. Li, A. Nag, A. C. Walters, M. Garcia-Fernandez, H. Robarts, M. Hashimoto, H. Lu, B. Nosarzewski, D. Song, H. Eisaki, Z.-X. Shen, B. Moritz, J. Zaanen, and T. P. Devereaux, “Spectroscopic Evidence for Charge Order Melting via Quantum Fluctuations in a Cuprate,” arXiv:2007.02464
- ⁵⁶ M. Le Tacon, A. Bosak, S. M. Souliou, G. Dellea, T. Loew, R. Heid, K.-P. Bohnen, G. Ghiringhelli, M. Krisch, and B. Keimer, Nature Physics **10**, 52 (2014).